Ore Geology Reviews 147 (2022) 104957

Contents lists available at ScienceDirect

Ore Geology Reviews

journal homepage: www.elsevier.com/locate/oregeorev

Sulphur and metal sources of polymetallic vein-type, sedimentary exhalative-type and Mississippi Valley-type Zn–Pb deposits along the southeast margin of the Yangtze Block

Zhengbing Zhou [a], Hanjie Wen [b,c,*], Jeffrey de Fourestier [a], Chaojian Qin [d], Ling Liu [e]

[a] State Key Laboratory of Nuclear Resources and Environment, East China University of Technology, Nanchang 330013, PR China
[b] School of Earth Science and Resources, Chang'an University, Xi'an 710054, PR China
[c] University of Chinese Academy of Sciences, Beijing 100049, PR China
[d] State Key Laboratory of Ore Deposit Geochemistry, Chinese Academy of Sciences, Guiyang 550081, PR China
[e] Geological Party 101, Guizhou Bureau of Geology and Minerals Exploration & Development, Kaili 556000, PR China

ARTICLE INFO

Keywords:
Southeast margin of the Yangtze Block
Zn–Pb deposit
Sulphur isotope
Lead isotope

ABSTRACT

Three types of zinc-lead deposits, including polymetallic vein-type, sedimentary-exhalative (SEDEX), and Mississippi valley-type (MVT) Zn–Pb deposits, have been discovered along the southeast margin of the Yangtze Block. A systematically comparative study on the sulphur and metal sources for these deposits, is absent, which significantly limits the understanding of the metallogenic model and geological exploration. Thus, in order to reveal the S and Pb sources of Pb–Zn deposits, an investigation of trace elements of sphalerite and of S–Pb isotopic compositions of sulphides in these three types of Zn–Pb deposits was conducted in this study. We found that, in the vein-type, SEDEX, and MVT Zn–Pb deposits, (1) the sulphur was derived respectively from granitic magmatism related to the Guangxi Orogeny, early Cambrian stratified seawater and connate water; (2) the lead isotope variation indicates that the ore-forming metals were mainly derived from the granitic hydrothermal fluids for vein-type deposits, from basement rocks for SEDEX deposits, and mainly from early Cambrian sedimentary rocks for MVT mineralization. The Nanhua rifting lead to the syngenetic Zn-Pb mineralization, while the Guangxi Orogeny resulted in magmatic-hydrothermal vein mineralization at depth and in MVT mineralization at the shallow crustal levels.

1. Introduction

Zinc-lead deposits are the primary hosts for base metals (Pb, Zn and Cu), as well as the most important repositories of critical minerals needed by the modern society, especially for In, Cd, Ge and Ga (Bauer et al., 2019; Schwarz-Schampera and Herzig, 2002; Wen et al., 2017; Werner et al., 2017; EU Commission, 2014; Marsh et al., 2016). Controlled by multi-stage tectonic events between blocks and/or plates, zinc–lead deposits tend to be concentrated in certain fields or mineralization belts (Hoggard et al., 2020). Some regions, such as the Carpentaria Zinc Belt in northern Australia, the Brooks Range in Alaska, the Selwyn Basin in Canada, the Chuan–Dian–Qian Zn-Pb mineralization field in China and Tennessee in the United States, contain large numbers of Zn-Pb deposits with various mineralization ages and different types (Goodfellow and Jonasson, 1984; Leach et al., 2005; Wilkinson, 2014; Hoggard et al., 2020). A deep understanding of the metallogenic mechanisms for magmatic–hydrothermal Zn–Pb deposits (Chang et al., 2019), SEDEX and MVT deposits (Machel et al., 1995; Bradley and Leach, 2003; Leach et al., 2005; Wilkinson, 2014) have been achieved. We usually regard that a remarkable metal enrichment sequence is required for the formation of a giant metal deposit, particularly in sediment-hosted deposits, such as sandstone Cu deposits, MVT and SEDEX Zn-Pb deposits and VHMS Cu-Zn-Pb deposits (Goodfellow and Jonasson, 1984; Leach et al., 2005; Ye et al., 2012; Wilkinson, 2014; Du et al., 2019). However, it is worth considering whether a remarkable metal enrichment sequence can provide sufficient metals for different types of deposits in the region. It is still unclear whether different types of lead–zinc deposits in the same mineralization field or belt, especially for sediment-hosted Zn–Pb deposits, have similar or entirely different metal and sulphur sources. This might have great influence on the

* Corresponding author at: School of Earth Science and Resources, Chang'an University, Xi'an 710054, PR China.
E-mail address: wenhanjie@vip.gyig.ac.cn (H. Wen).

https://doi.org/10.1016/j.oregeorev.2022.104957
Received 3 January 2022; Received in revised form 23 May 2022; Accepted 26 May 2022
Available online 28 May 2022

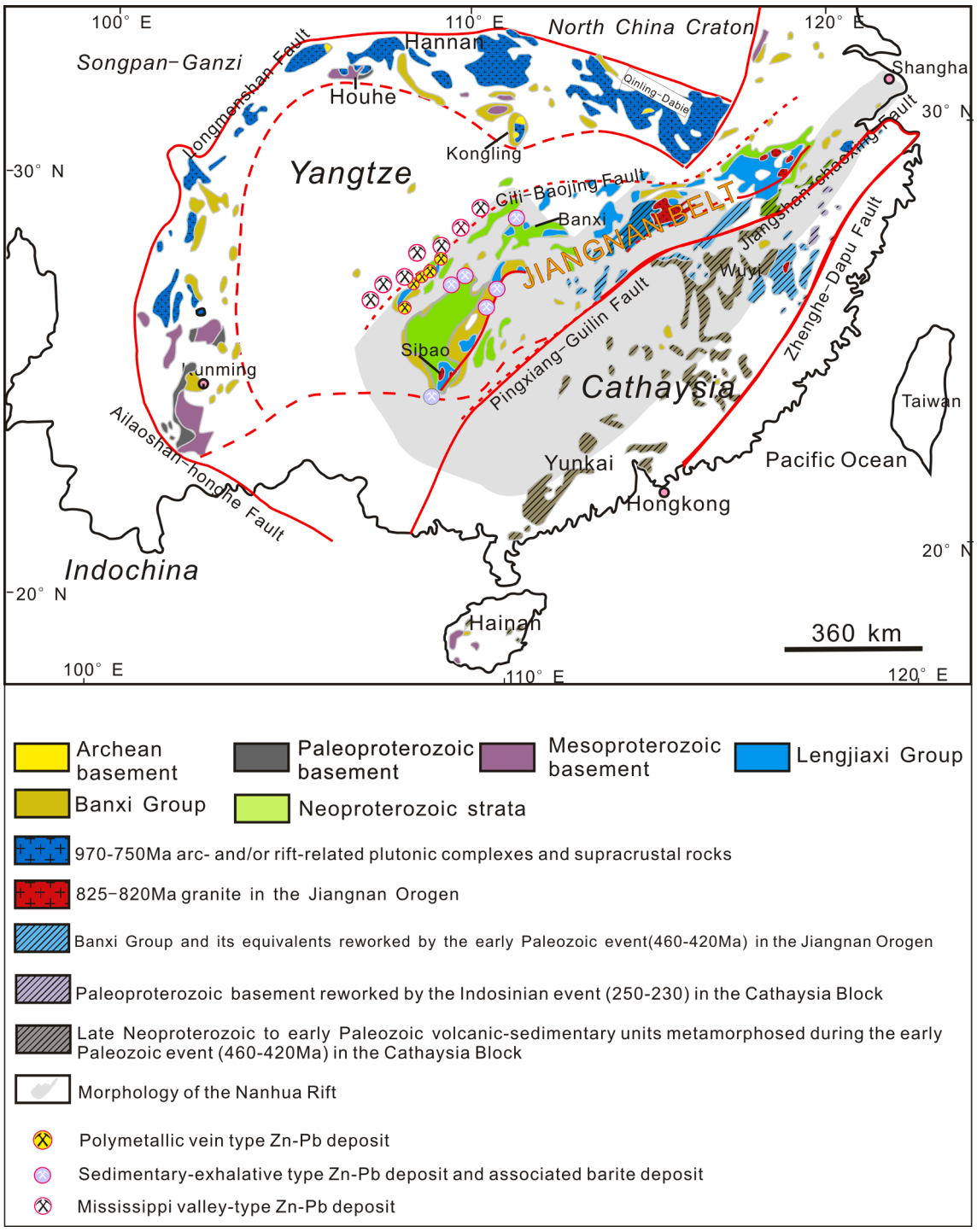

Fig. 1. Regional geological setting and the location of southeast margin of Yangtze Block, showing the location of major zinc-lead deposits (modified from Zhao, 2015; Su et al., 2017; Zhou and Wen, 2021).

interpretation or recognition of the metallogenic model, especially in a mineralization field with various types of Zn–Pb deposits.

Numerous Zn-Pb deposits have been described from the southeast margin of the Yangtze Block. Three types of Zn-Pb mineralization have been distinguished: (1) polymetallic vein type occurring in the sandstone and siltstone of the Banxi Group (Zhou et al., 2017); (2) sedimentary-exhalative (SEDEX) type hosted within dolomite and shale of the Doushantuo and Niutitang (Wen et al., 2017; Zhou et al., 2018); and (3) Mississippi valley type (MVT) hosted within carbonate sediments of middle Cambrian to early Ordovician age (Schneider et al., 2002; Ye et al., 2012; Cai et al., 2015). Additionally, the tectonic evolution history of the southeast margin of the Yangtze Block have been clearly identified. Specifically, during the late Ediacaran to early Cambrian, this region underwent episodic rifting, and intensive fault depressions in the Nanhua Basin resulted in intensive hydrothermal exhalative sediments (Feng et al., 2010; Zhang et al., 2013a,b). Rifting event ended by the Guangxi intracontinental orogeny (ca. 462–396 Ma) (Wang et al., 2012), which had induced relatively strong thrust deformation on the Xuefeng uplift (Jin, 2010). Previous works have realized that the SEDEX ores formed during rifting events in the early Cambrian

stage (Zhou et al., 2018); the polymetallic vein-type and MVT Zn–Pb mineralization were formed in the period of the Guangxi Orogeny (Zhou et al., 2017). Moreover, in the Phanerozoic, metamorphism was weak along the southwest margin of the Yangtze Block (Wang et al., 2012; Zhang et al., 2013a,b). No intense post-ore alteration textures have been found in these deposits, thus ruling out the possibility of remobilization of one ore to form another. Therefore, the southeast margin of the Yangtze Block is an ideal place to determine if different types of lead–zinc deposits in the same mineralization field, have similar or entirely different metal and sulphur sources.

Here we report data pertaining to the geology, trace element concentrations of sphalerite and S–Pb isotopic compositions of the three types of Zn–Pb deposits at the southeast margin of the Yangtze Block. Meanwhile, this study provides insight into metal sources, sulphur sources, and mechanisms of mineralization. Based on these data, the possible and controlling factors for the metal and sulphur sources in the mineralizing process are further discussed, which could appear to be critical for understanding the ore formation processes in Zn–Pb mineralization fields.

2. Regional geological setting

The Yangtze Block and Cathaysia Block are generally considered to record polyorogenic evolution involving the stacking of Proterozoic microplates in the Mesoproterozoic.

The South China Block comprises the Yangtze Block, the Cathaysia Block, and the Jiangnan Orogen between them (Fig. 1). During 970–825 Ma, the Paleo-Huanan oceanic lithosphere underwent divergent double subduction beneath both the southeastern margin of the Yangtze Block and the northwestern margin of the Cathaysia Block (Zhao, 2015), accompanied by sedimentation of sandstone, siltstone, and slate with minor tuff (with occurrences of spilite, keratophyre, and komatiitic), which were uniformly assigned to the Lengjiaxi Group (Wang et al., 2004, 2008; Zhao and Cawood, 2012; Zhou et al., 2017). Then, the Yangtze Block and the Cathaysia Block collided along the two overriding continental margins during the Jinning Orogeny (ca. 825–815 Ma) and formed the Jiangnan Orogen (Fig. 1) (Li et al., 1999; Li et al., 2003; Zhao and Cawood, 2012; Zhang et al., 2013a,b). Strata of the Lengjiaxi Group are characterized by high-angle upright folds induced by this orogeny (Li et al., 1999; Zhang et al., 2013a,b).

Between ca. 815 Ma and 420 Ma, during the breakup of the supercontinent Rodinia, regions along the Jiangnan Orogen experienced episodic rifting (Feng et al., 2010; Zhang et al., 2013a,b) and a southeast-facing passive continental margin developed on the Yangtze Block throughout the rifting (Fig. 1) (Wang and Li, 2003). During this period, the sedimentary sequences in ascending order were: (1) the Neoproterozoic Banxi Group, with a maximum thickness of 7000 m, built up by low-grade metamorphosed sandstone, siltstone and minor tuff interbeds; (2) the Neoproterozoic Nanhua and Ediacaran systems, composed of glacial–interglacial sediment suites. (3) the Cambrian system, mainly containing micrite or algae-bearing carbonates, chert and shales. Rifting events were eventually ended by the Guangxi intracontinental orogeny (ca. 462–392 Ma), which allowed for second collision of the Yangtze and Cathaysia Blocks and a final reunion of the South China Plate (Charvet et al., 2010; Shu, 2012; Zhang et al., 2013a, b; Chen et al., 2010, 2012; Wang and Li, 2003; Zhou et al., 2017). The Guangxi intracontinental orogeny resulted in an extensive foreland basin along the southeast margin of the Yangtze Block (Jin, 2010) and few lamproites (ca. 503–438 Ma) intrude into Cambrian sedimentary rocks (Mei et al., 1998; Fang et al., 2002). In the southern region of the conjunction zone of the Yangtze Block and the Jiangnan Orogen, voluminous plutons were emplaced in the post-collisional tectonic setting from ca. 400 to 464 Ma (peaking at ca. 420–446 Ma; represented by Baimashan and Miao'ershan plutons) (Bai et al., 2015; Chen et al., 2016).

The Indosinian collision (between ca. 270 and 208 Ma) was another Phanerozoic intracontinental orogeny in the South China Block (Zhang et al., 2013a,b; Wang and Li, 2003). This collision resulted in intense magmatism and metamorphism in the eastern part of the South China Block. In contrast, the southeast margin of the Yangtze Block was only subjected to slight structural deformation at the shallow crust scale (Jin, 2010; Zhang et al., 2013a,b; Wang and Li, 2003; Li et al., 2015a, b, 2016).

Table 1
Comparison of principal characteristics of Polymetallic vein type, SEDEX and MVT deposit in the southeast margin of Yangtze Block.

Characteristics	Polymetallic vein type	SEDEX	MVT
Host rock	Banxi Group; sandstone, siltstone	Doushantuo Formation; carbonates and shales	Qinxudong Formation; limestones
Structural controls	Fault-bound	Fault-bound and stratabound	Stratabound
Morphology of orebodies	Vein	Vein, layered, lenticular	Vein, massive, lamellar-lenticular
Major alteration	Silicification	Silification, carbonate alteration	Carbonate alteration
Ore minerals	Sph, Gn, Ccp, Py	Sph, Py, Mrc, Gn	Sph, Gn, Py, Mrc, trace amounts of Ja
Gangue minerals	Qz, Cal	Brt, Qz, minor Bit, Cal, Ap, Hy	Cal, Dol, Brt, Qz, Bit, Flr
Metal association	Zn, Pb, Cu, Fe, In	Zn, Fe, Pb, Ba	Zn, Pb, Fe
Grades	Zn 3.8–25.1%, Pb 0.4–5.6%, Cu 0.1–5.8%	Zn 0.9–10.2 %, Pb 1.2–1.4 %	Zn 3.9%, Pb 1.4%
Ore-forming fluid	Magmatic-related hydrothermal fluids	Brines	Basinal brine
Timing of mineralization	462–396 Ma	541–516 Ma	480–410 Ma
Tectonic setting	Orogeny	Rift basin	Foreland basin
Typical deposit	Jinbao metallogenic district (Aihe, Bengchong, Laodu and Pingmen deposits), Nansun metallogenic district (Nansun and Paiwang deposits), Yangjiawan and Miaoniao deposits	Dongjiahe, Dilu, Laobao, Dahebian	Longshan orefield, Aoxi orefield, Huayuan orefield Panshi deposit, Xiunao, Bokouchang, Yebadong, Longjinjie, and Niujiaotang deposit

The Abbreviation: Sph-sphalerite; Gn-Galena; Py-Pyrite; Ccp-Chalcopyrite; Mrc-Marcasite; Ja-Jamesonite; Qz-Quartz; Cal-Calcitie; Dol-Dolomite; Ap-Apatite; Hy-Hyalophane; Brt-Barite; Bit-Bitumen; Flr-Fluorite.

3. Ore geology

3.1. Polymetallic vein-type deposits

Polymetallic vein-type Zn-Pb deposits are mainly hosted in the Pinglue Formation and the Qinshuijiang Formation, belonging to the upper part of the Banxi Group. Host rocks chiefly consist of low-grade metamorphic sandstone, siltstone with minor tuff interbeds (Table 1; Zhou et al., 2017). Ore is mainly found in fault-bounded quartz veins (Fig. 2) and primarily contains sphalerite, galena, chalcopyrite and pyrite, accompanied by quartz and minor calcite (Fig. 5a,c,e,f). In the vein-type deposits, lamellar and micro-veined chalcopyrite appeared to be distributed in double-crystal joints and cracks of sphalerite (Fig. 5f). Mineralization accompanied with intensive silicification (Fig. 5b,c,e), carbonate alteration can be found at the relative higher part. Four mineralization stages can be distinguished: (1) the silicification stage is represented by massive euhedral granular quartz (Fig. 5b, c); (2) the Zn-Pb-Fe sulfides stage, dominated by coarse-grained black sphalerite,

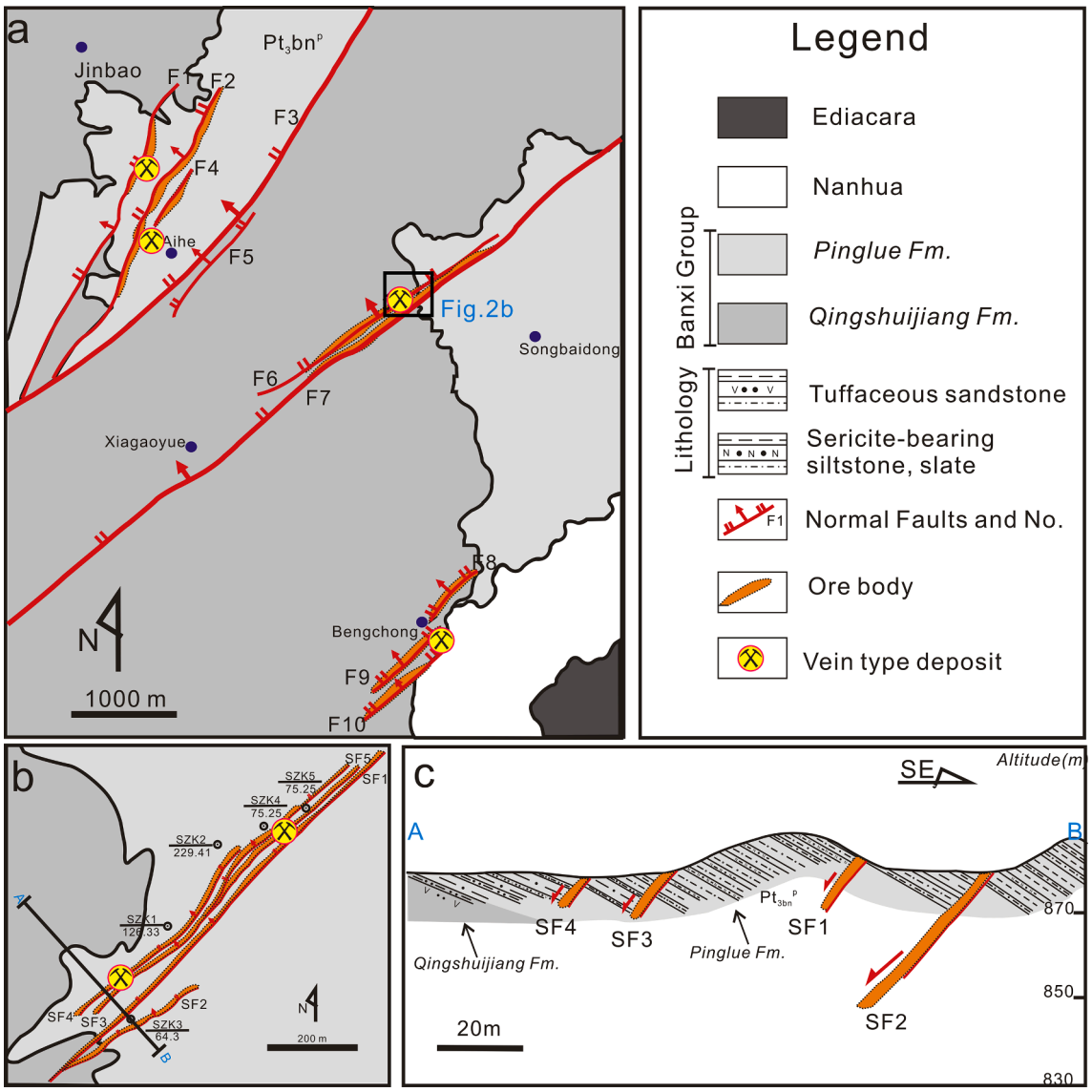

Fig. 2. a. Geological map of the Jinbao metallogenic district; b. Geological map of the Songbaidong deposit in the central of Jinbao metallogenic district; line AB is the location of the cross-section shown on (c); c. the cross-section through Songbaidong deposit, showing mineralization of typical polymetallic vein-type deposits (modified from Zhou et al., 2017).

coarse-grained galena and pyrite (Fig. 5b, c, d); (3) Zn-(In)-Cu-Pb sulphide stage, where fine-grained pale-yellow to light brown sphalerite, chalcopyrite, and galena are deposited with fine-grained quartz and calcite (Fig. 5d, e, f); and lastly, (4) post-sulphide stage with minor amounts of chalcedony and calcite veinlets.

Active polymetallic vein-type mines include the Jinbao metallogenic district (Aihe, Bengchong, Laodu and Pingmen deposits), the Nansun metallogenic district (Nansun and Paiwang deposits), the Yangjiawan and Miaoniao deposits (Zhou et al., 2017). The mineralization is dominated by zinc and lead, accompanied by various concentrations of copper. Zn, Pb and Cu grades of ores are 3.8–25.1%, 0.4–5.6%, and 0.1–5.8%, respectively (Zhou and Wen, 2021). However, due to the low level of exploration, the reserve has not been clearly assessed (Zhou and Wen, 2021).

Zhou et al. (2017, 2020) and Xu et al. (2018) proposed that these deposits were possibly stemmed from a magmatic-related hydrothermal system, based on their geochemical signatures (fluid inclusions, and C-H-O-Pb-Li-Cd-Zn isotopic variations). They put forward a plausible model of magmatic-related hydrothermal system ascending along faults and emplacement into open space mixing with meteoric water, in response to cooling and boiling of magmatic hydrothermal fluids. These processes resulted in the wide range of temperatures and salinity for hydrothermal fluids: the homogenization temperature and salinity of fluid inclusions are in the range of 87–262 °C and 2.73–26.64 wt% NaCleqv., respectively (Zhou et al., 2017).

3.2. SEDEX deposits

SEDEX Zn-Pb deposits are hosted in the Doushantuo Formation, Liuchapo Formation and Niutitang Formation, that consist of carbonates sediments and shales (Table 1; Zhou et al., 2018). Ore can be separated into two types: (1) the replacement ore in the recharge zone, mainly discordant but stratabound in the Doushantuo Formation (Fig. 3); (2) stratiform barite ore and laminated sulphide layer in the Niutitang Formation (Fig. 5g; Wen et al., 2017; Zhou et al., 2018). The sulphide ore consists primarily of sphalerite, pyrite, marcasite and galena, associated with barite, quartz, minor bitumen and calcite, as well as trace amounts of apatite and hyalophane (Fig. 5j-l). Minor chalcopyrite occurred as “chalcopyrite disease” texture in some sphalerite (Fig. 5 l). Sulphide mineralization is usually related to intensive brecciation in the

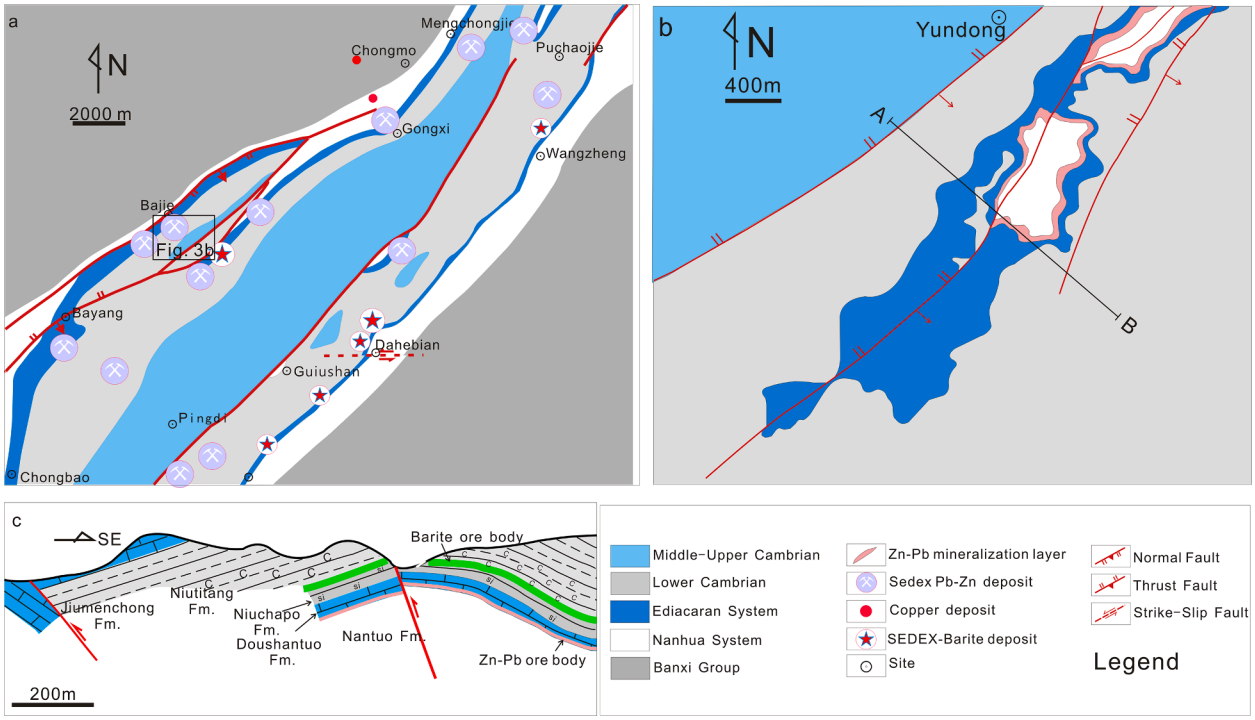

Fig. 3. a. Geological map of the Dahebian district, showing locations of zinc-lead deposits and stratiform barite deposits (modified from Zhou et al., 2018); b. Geological map of the Yundong Zn-Pb deposit in the northwestern Dahebian district; line AB is the location of the cross-section shown on (c); c. Representative cross-section in the Dahebian district, showing the SEDEX mineralization patterns.

host-rocks (Fig. 5h), accompanied by silification, and associated with barite and carbonate (Fig. 5k, l; Zhou et al., 2018). The hydrothermal history of SEDEX deposit can be divided into three stages: (1) Fe-Zn sulphide stage is precipitated with massive coarse-cubic pyrite and red-brown sphalerite. Gauge minerals are composed of quartz and dolomite, accompanied with bitumen, minor amounts of apatite and hyalophane; (2) Zn-Fe-Pb sulphide stage is represented by fine-grained pyrite, pale-yellow sphalerite and minor amounts of galena and acicular marcasite (Fig. 5k, j). Sulfides mainly co-precipitated with quartz, bitumen, barite, minor amounts of hyalophane. Sphalerite and pyrite particles display mosaic pattern in bitumen (Zhou et al., 2018). (3) Barite stage, where barite and minor amounts of sulphide mineral, witherite and dolomite precipitated as veinlets (Fig. 5h).

The Dongjiahe, Dilu and Laobao Zn-Pb deposits have been mined since the 1990s (Luo, 1990; Zeng and Li, 2007; Liang et al., 2009; Liao et al., 2013; Xiang and Luo, 2013; Wen et al., 2017). The Dahebian Zn-Pb deposit is a newly discovered deposit, containing >0.5 Mt Pb + Zn reserve with grade of 0.91–10.15% Zn and 1.24–1.36% Pb (Wen et al., 2017).

The homogenization temperature and salinity of fluid inclusions are in the range of 142–368 °C, from 0.53 to 25.62 wt% NaCleqv., respectively (Zhou et al., 2018). Wen et al. (2017) and Zhou et al. (2018) proposed that these deposits were possibly arisen from Selwyn-Type sedimentary exhalative hydrothermal fluids. Also, Zhou et al. (2018) consider that Zn-Pb sulphides were mineralized in the recharge zone of these hydrothermal fluids, and the stratiform barite ore deposits represent the upper sedimentary-exhalative mineralization. Actually, the basal areas of the Niutitang Formation deposition recorded intensive exhalative processes by hydrothermal fluids during the rifting of the Nanhua Basin. For example, the stratiform phosphorite and barite units, sapropelite (thickness up to tens of metres), and an organic matter- and sulphide-rich Ni-Mo-PGE ore layer are widespread along the southeast margin of Yangtze Block (Jiang et al., 2006; Wen and Carignan, 2011; Zhou et al., 2018).

3.3. MVT deposits

MVT Zn-Pb deposits are mainly hosted in the Qinxudong Formation that consists of largely cyanobacterial mound limestones and oolitic intramound limestones (Table 1; Fig. 4), although some deposits are hosted in the Nanjinguan formation, which consists of nodular and bioclastic limestones and interbedded with carbonaceous shale. The mineralization field mostly shows a replacement texture and occurs as veins, massive or as lamellar-lenticular ores (Fig. 5m, n). Ores primarily contain sphalerite, accompanied by galena and pyrite. Trace amounts of marcasite and jamesonite have been found in the Limei deposit (Cai et al., 2015). Sphalerite is relatively clean with rare chalcopyrite inclusions (Fig. 5r). Gangue minerals are chiefly calcite and dolomite (Fig. 5m-o), associated with barite (Fig. 5o, p), quartz, bitumen and fluorite (Fig. 5p). Wall-rock alteration at MVT deposits introduced calcite, organic matter, and fluorite with minor quartz and dolomite. The paragenetic sequence can be divided into three stages: (1) Fe-Zn sulphide stage consisting of abundant euhedral pyrite and porous sphalerite, accompanied by minor calcite; (2) Pb-Zn-Fe sulphide stage, where sphalerite and galena are the main sulfide minerals, with minor amounts of fine-grained pyrite. Sulfide minerals are commonly co-precipitated with calcite, dolomite and bitumen (Fig. 5n, q); (3) Post-sulphide stage, represented by dolomite, calcite, fluorite, and barite (Fig. 5o, p).

MVT Zn-Pb deposits are the main mining resources in the southeast margin of Yangtze Block. At present, dozens of lead–zinc deposits (points) of different sizes have been discovered, with Longshan orefield, Aoxi orefield and Huayuan orefield in western Hunan, Panshi deposit, Xiunao, Bokouchang, Yebadong, Longjinjie, and Niujiaotang deposit in the eastern Guizhou. MVT deposits contain >20 Mt Zn + Pb reserves with an average ore grade of 3.93% Zn and 1.40% Pb (Zhou et al., 2018; Ye et al., 2018).

The homogenization temperatures of fluid inclusions mostly fall in the range of 110–130 °C with a salinity beyond 10 wt% NaCleqv. (Ye et al., 2018). To date discovered deposits occur in the foreland basin that

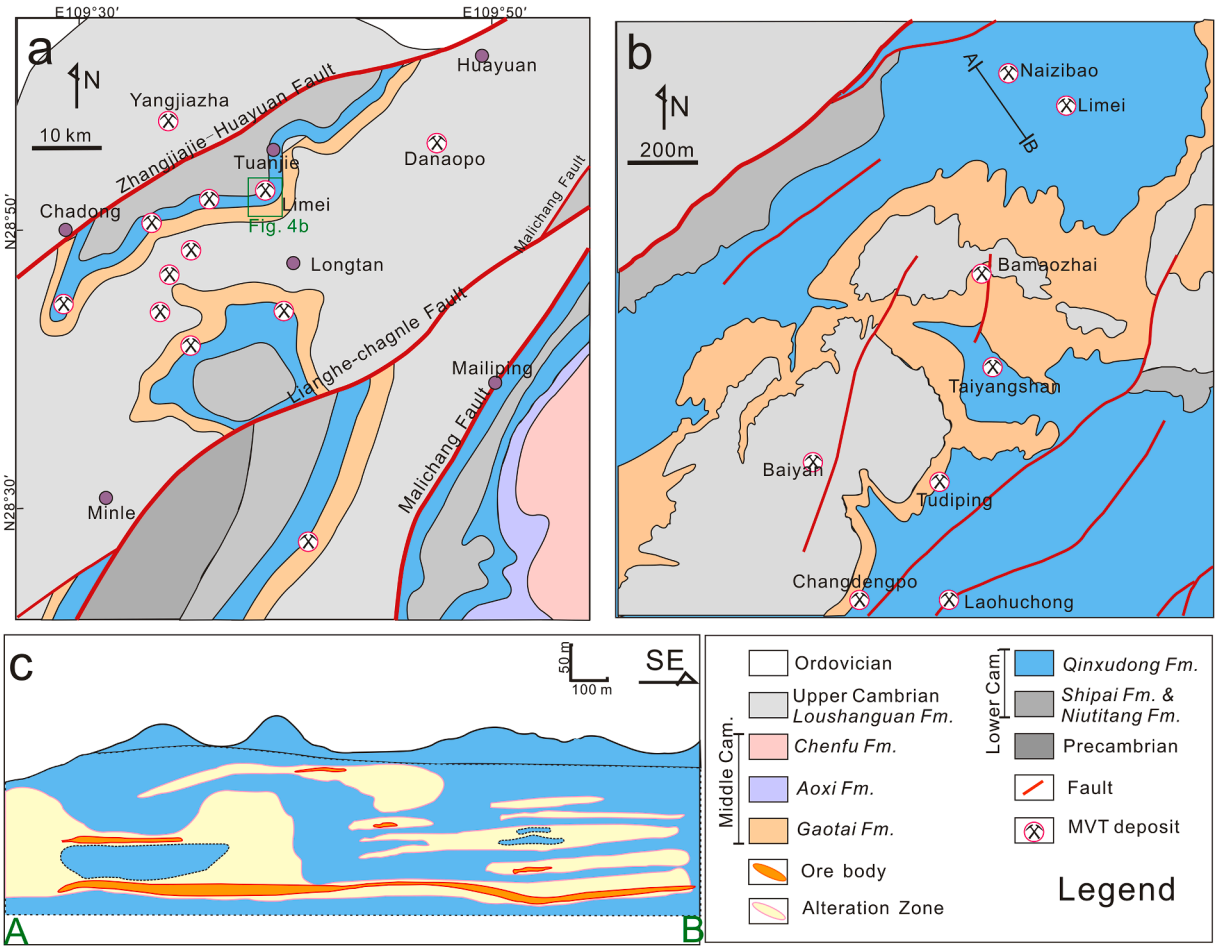

Fig. 4. a. Geological map of the Huayuan deposit and showing the distribution of Pb-Zn deposits (modified from Duan, 2014); b. Geological map of the Limei Zn-Pb deposit; line AB is the location of the cross-section shown on (c); c. the cross-section through the Limei deposit, showing the distribution of the sulfide ores and alteration zones (modified from Zhou, 2017).

formed during the Guangxi orogeny (Jin, 2010; Ye et al., 2012; Cai et al., 2003; Wu et al., 2019). Lead-zinc mineralization is closely related to ancient oil reservoirs (Ye et al., 2018). Most MVT deposits in this region occurred in the foreland basin that also formed during the Guangxi orogeny (Jin, 2010; Wu et al., 2019; Ye et al., 2012; Cai et al., 2015). The geological and geochemical characteristics of this mineralization are similar to typical MVT Zn-Pb deposits (Leach et al., 2005; Wilkinson, 2014; Ye et al., 2018).

4. Samples and methodology

In order to investigate sulphur and metal source, trace elements contents, sulfur and lead isotope data from Zn-Pb deposits from the southeast margin of Yangtze Block were compiled in this study from a wide number of publications (Schneider et al., 2002; 15 Duan, 2014; Liang, 1989; Luo, 1990; Ye et al., 2012; Zhou, 2017; Zhou et al., 2017, 2018; Liu and Zhu, 1994; Xia et al., 2004; Cai et al., 2015; Hu et al., 2017; Zhou and Wen, 2021). Also, based on recently discoveries in mining and exploration works, we collected samples to measure trace element concentrations and S-Pb isotopic compositions, to ensure the comprehensive and reliable of data. Representative samples were crushed into 40–80 mesh, to selected sulphides by handpicking using a binocular microscope. These sulphides samples were then crushed to 200 mesh using an agate mortar.

The detailed methodology for analysis is described below:

(1) Element concentrations: Twenty-one sphalerite samples from the Dahebian deposit (SEDEX type) were selected for element concentration measure, which were carried out at the State Key Laboratory of Ore Deposit Geochemistry, Institute of Geochemistry, Chinese Academy of Sciences (SKLODG). Overall, 30 mg of sphalerite was weighted in a Teflon beaker and digested by means of a microwave digestion technique. Zn, Fe, Cu, Cd, Ga, Ge, In, Tl and Se concentrations were measured with an inductively coupled plasma optical emission spectrometer (ICP-OES; Varian Vista MPX). The relative standard deviations were typically lower than 10%.

(2) Sulfur isotope: fourteen sphalerite samples, seven pyrite samples, seven galena samples and two barite samples from SEDEX deposit (Dongjiahe, Dilu and Laobao deposit), and twenty-five sphalerite samples, three pyrite samples, eight galena samples from MVT deposit (Yutang, Limei, Tuanjie, and Duping), two galena samples and four chalcopyrite samples from the vein type deposit (Pinmen) were prepared for sulfur isotopic analysis. Sulphur isotope analysis was carried out using an EA-MAT-253 mass spectrometer at SKLODG. The SO_2 which was used for the gas mass spectrometer measurements, was produced through sulphides combusted with copper oxide under vacuum at 1000 °C (Robinson and Kusakabe, 1975). Isotopic data were reported as $\delta^{34}S$ relative to CDT. IAEA-S-1 ($\delta^{34}S_{VCDT} = -0.30‰$), IAEA-S-2 ($\delta^{34}S_{VCDT} = 22.62‰$) and IAEA-S-3 ($\delta^{34}S_{VCDT} = -32.49‰$) were measured as internal standards. The relative error at 2σ was better than 0.1‰.

(1) Polymetallic vein type deposit

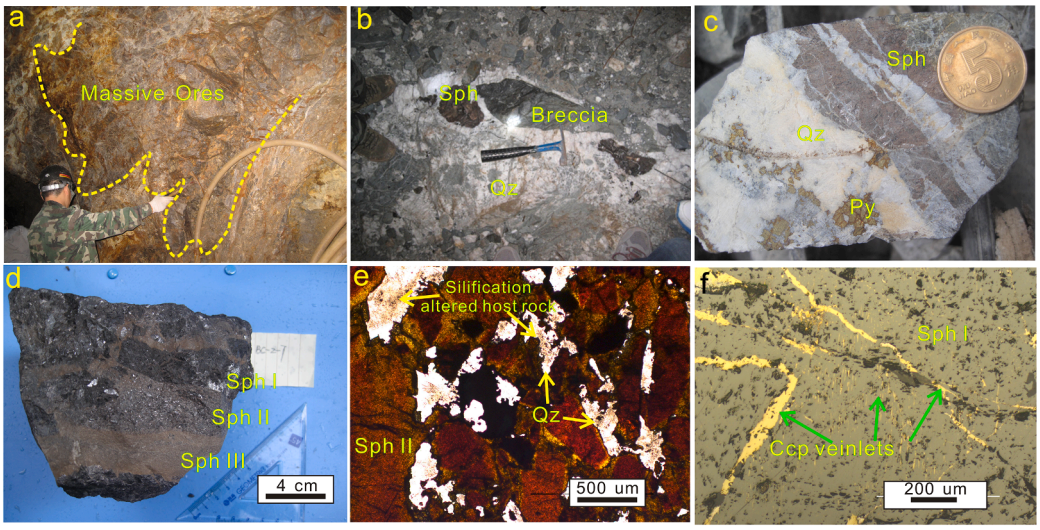

(2) SEDEX deposit

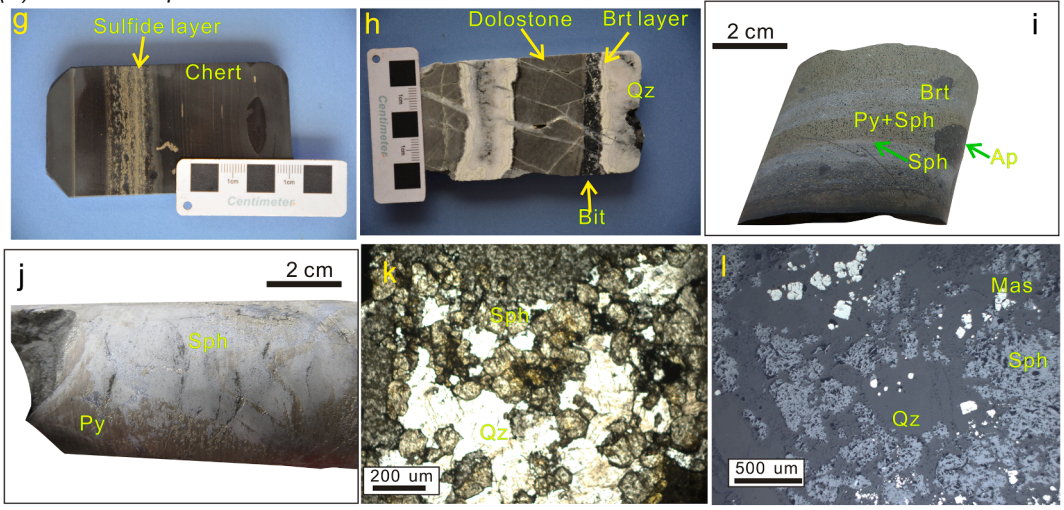

(3) MVT deposit

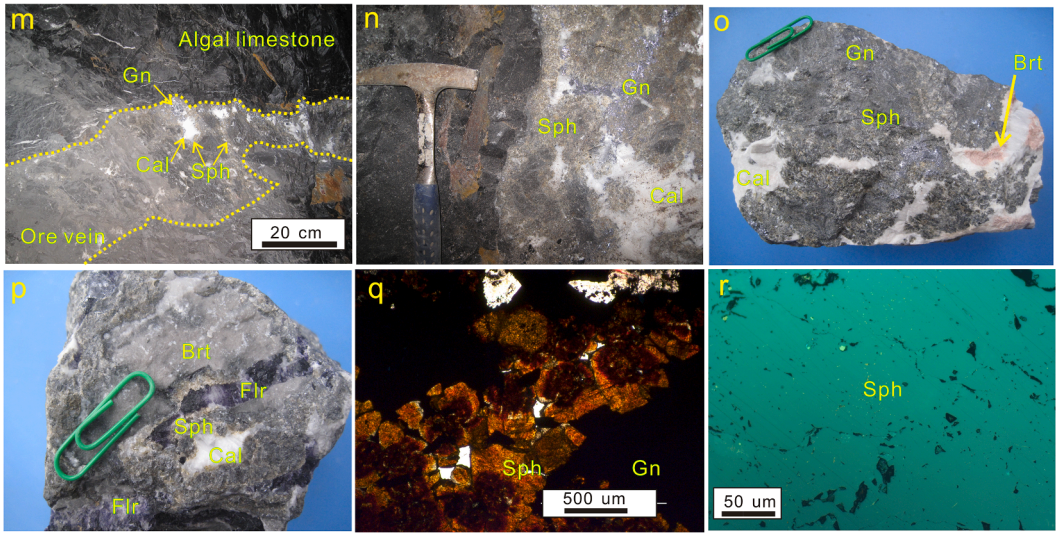

(caption on next page)

Fig. 5. Mineralization features in the metal-bearing veins and ores. Polymetallic vein Ores showing: (a) massive ore; (b) and (c) Ore veins fill in the fracture of host rock; (d) fine grained sphalerite overlap on early stage's coarse grained sphalerite; (e) brownish red sphalerite inter-growth with quartz; (f) vein-like and bladed chalcopyrite distributed in the fracture and double-crystal joint of sphalerite (Zhou et al., 2017). (For interpretation of the references to colour in this figure legend, the reader is referred to the web version of this article.)

SEDEX ores showing: (g) and (i) laminated pyrite and sphalerite; (h) barite and bitumen replaced dolostone of the Doushantuo Formation; (j) fine grained sphalerite and calcite filling interspaces between early stage course grained pyrite; (k) pale-yellow sphalerite intergrowth with quartz; (l) sphalerite intergrowth with quartz and marcasite. MVT ores showing: (m) and (n) ore veins interbedded through algal limestone of the Qinxudong Formation; (o) Cockade sphalerite and barite; (p) sphalerite intergrowth with calcite, barite and fluorite; (q) brownish and red sphalerite inter-growth with dolomite; (r) relatively clear sphalerite. Photos a-d, g-j, and m-p were taken under sunlight; e, k, and q were taken under transmitted plane-polarized light; f, l, and r were taken under reflected plane-polarized light.Abbreviations: *Sph* sphalerite; Gn galena; *Ccp* chalcopyrite; *Py* pyrite; *Mas* Marcasite; *Qz* quartz; *Brt* Barite; *Cal* Calcite; *Bit* Bitumen; *Flr* Fluorite.

(3) Five fresh and unaltered basement rock samples were collected from a section of newly excavated road in the Leishan County, Guizhou Province, to measure lead isotopic compositions, which were performed at the State Key Laboratory of Nuclear Resources and Environment. Lead was separated and purified by using cation-exchange technique. Diluted HBr was selected as the eluent (Zhou et al., 2017). Isotopic Pb ratios were analyzed using a *Thermo-Scientific Neptune plus* MC-ICP-MS coupled with a membrane desolvation system (*CETAC Aridus II*). Lead isotopes are reported relative to the measured ratio of NBS981 ($^{206}Pb/^{204}Pb = 16.9327 \pm 0.0002$, $^{207}Pb/^{204}Pb = 15.4843 \pm 0.0004$, and $^{208}Pb/^{204}Pb = 36.6856 \pm 0.0001$; Zhou et al., 2018), and instrumental mass bias correction was adopted through Tl-doping method. The precision of $^{208}Pb/^{206}Pb$ measurements (1 μg of Pb) is better than 0.001%.

5. Results

5.1. Trace element variations of sphalerite

Trace elements of sphalerite, especially chalcophile elements, are listed in Appendix B, summarized with mean and standard deviation values in Table 2 and shown in Fig. 6 and Fig. 7.

The vein sphalerites display relatively higher Co, In, Sn, Fe, Cu, Mn, Ga and Se contents compared to the MVT and SEDEX sphalerites in this region. The main characteristic of vein type sphalerite is the large amount of Fe, Cu, and In, mostly above 45,000 ppm, 1478 ppm, and 38 ppm, respectively (Fig. 6). Also, variations in concentration are relatively minor in Cr, Co, Sn, Ge, Ag, and Sb compared to Fe, Cu, Mn, Pb, or Cd with large disparities.

In SEDEX sphalerite, the Cr, V, Ge, As and Ni content is relatively higher than others sphalerite. Indium and Ge content are generally below the detection limit, while Ge detected mean values in the Tianzhu deposit and Laobao deposit are 78.4 ± 107.5 ppm (Fig. 6). In addition, the Cr, Co, Sn, Fe, Cu, Cd, Mn, and Se contents are fall in between the vein type and MVT type (Fig. 6).

The MVT sphalerites have the higher Cd and Ge contents but the lowest Co, In, Sn, Fe, Cu, Mn, Se, Ni and Sb contents. Cadmium and Fe contents show generally large variations from 956.6 to 26998.0 ppm for Cd and from 985 to 77235 ppm for Fe. Germanium content is slightly higher from the Niujiaotang deposit with a mean value of 82.39 ± 117.04 ppm. Sphalerite Tl values are typically <3 ppm in all SEDEX and vein type deposits, but a few MVT sphalerites have detectable Tl concentrations, the highest value in this study is 43.60 ppm.

5.2. Sulphur isotopes

$\delta^{34}S_{VCDT}$ values of sulphides (sphalerite, galena, pyrite, and chalcopyrite) and sulphate (barite) selected from Zn–Pb deposits along the southeast margin of the Yangtze Block are listed in Table 3 and Appendix C. Sulphide samples showed a narrow range of $\delta^{34}S_{VCDT}$ values for polymetallic vein deposits, from 8.8‰ to 14.4‰. In contrast, sulphide samples indicated a relatively broad range of $\delta^{34}S_{VCDT}$ values with a range of −17.4‰ to 30.0‰ (average 14.0‰, n = 102). The $\delta^{34}S_{VCDT}$ values of sulphides from MVT Zn–Pb deposits ranged from 20.3‰ to 37.2‰ (average 30.4‰, n = 115). Barite from SEDEX and MVT deposits had $\delta^{34}S_{VCDT}$ values of 29.5‰–48.3‰ and 31.3‰–42.0‰ respectively.

5.3. Lead isotopes

Lead isotopic compositions of sulphides from the Zn–Pb deposits, together with early Cambrian sediments and the basement rocks from the southeast margin of the Yangtze Block, are summarized in Table 4 (detail data in Appendix D)and shown in Fig. 10 and Fig. 11.

The sulphides of the vein-type deposits have relatively smaller ranges of $^{206}Pb/^{204}Pb$ (17.139–17.258), $^{207}Pb/^{204}Pb$ (15.432–15.508) and $^{208}Pb/^{204}Pb$ (37.282–37.546). Sulphides of SEDEX ores are confined to a range of $^{206}Pb/^{204}Pb$ ratios from 17.597 to 17.750, $^{207}Pb/^{204}Pb$ ratios from 15.537 to 15.586, and $^{208}Pb/^{204}Pb$ ratios from 37.587 to 37.801. MVT deposits have high and heterogeneous radiogenic lead isotopic compositions. The $^{206}Pb/^{204}Pb$ ratios, $^{207}Pb/^{204}Pb$ ratios, and $^{208}Pb/^{204}Pb$ ratios are in the range of 18.028–18.266, 15.621–15.875, and 38.099–38.888, respectively. Moreover, the $^{206}Pb/^{204}Pb$ ratios are positive related with $^{207}Pb/^{204}Pb$ and $^{208}Pb/^{204}Pb$ (Fig. 10).

Basement rocks in this region show considerable spread of lead isotopic values. The ratios of $^{206}Pb/^{204}Pb$, $^{207}Pb/^{204}Pb$, and $^{208}Pb/^{204}Pb$ range from 17.507 to 22.038, 15.430 to 15.937, and 37.876 to 46.917, respectively. The Niutitang, Liuchapo and Qingxudong formations have ranges of $^{206}Pb/^{204}Pb$ ratios from 16.345 to 18.817, 17.559 to 18.484, and 18.067 to 19.073, respectively; $^{207}Pb/^{204}Pb$ ratios ranging from 15.486 to 15.721, 15.636 to 15.686, and 15.626 to 15.783, respectively; and ranges of $^{208}Pb/^{204}Pb$ ratios from 37.369 to 38.619, 37.919 to 38.343, and 38.107 to 39.408, respectively.

6. Discussion

6.1. Different trace and minor element assemblages in sphalerite

Specific ranges of trace element concentrations, such as In, Ga, Ge and Cd, in sphalerite from different types of deposits have been observed in numerous previous works (Cook et al., 2009; Cugerone et al., 2019; Gagnevin et al., 2014; Wen et al., 2016a,b; Ye et al., 2011; Xu et al., 2020). Based on trace element data, we can obtain the physico-chemical conditions (temperature and fs_2) during the sphalerite formation processes (Cook et al., 2009; Frenzel et al., 2016a,b, 2022; Ye et al., 2012; Cugerone et al., 2019). Additionally, sphalerite is one of the most important carriers for critical elements (Wen et al., 2019). Indium, Ge and Cd concentrations in sphalerite can reach up to $n \times 10^4$ ppm (Murakami and Ishihara, 2013), $n \times 10^3$ ppm (Cugerone et al., 2019) and $n \times 10^5$ppm (Wen et al., 2016a), respectively. Sphalerites in polymetallic vein, SEDEX, and MVT deposits along the southeast margin of the Yangtze Block display varying trace element composition characteristics (Figs. 6, 7). In the binary diagrams of Zn/Cd–In, Cd–Co and Fe-Mn, three types of deposits appeared at relatively independent intervals (Fig. 7).

Compared with SEDEX and MVT sphalerites, the vein sphalerite has relatively higher Co, In, Sn, Fe, Cu, Mn and Se content but the lowest Cd, Tl, Ni contents. Many studies have demonstrated that, in general, high-

Table 2
Summary of trace element concentrations for sphalerite in different deposit types in the southeast margin of Yangtze Block (ppm).

Deposit type		Cr	Co	V	Sn	Fe	Cu	In	Cd	Ga	Ge	Mn	Pb	Ag	As	Sb	Se	Tl	Ni
Polymetallic vein deposit																			
	Max	6.8	282.0	7.6	155.3	64,443	5314.3	189.5	3275.0	366.4	31.3	1191.4	2305.0	11.4	52.5	44.1	42.9	–	29.54
	Min	0.3	18.0	0.5	4.8	26,397	442.6	2.0	864.6	74.3	4.0	111.4	17.6	1.4	4.3	0.9	7.5	–	0.40
n = 25	Mean	1.5	92.3	1.8	40.5	46,769	1478.3	38.1	1815.7	189.9	8.6	337.2	323.5	5.4	13.1	11.1	21.3	–	4.26
	s.d	1.9	82.9	2.3	46.8	12,606	1411.3	44.3	674.1	82.7	7.6	294.2	508.9	2.3	13.1	13.1	11.9	–	7.61
SEDEX deposit																			
	Max	134.7	4.6	8.2	5.9	39,082	952.3	–	14727.3	19.4	202.3	507.7	2705.7	18.3	65.9	43.88	19.74	3.06	255.10
	Min	0.5	0.9	0.9	0.9	3311	80.1	–	4112.2	1.1	10.2	39.6	39.8	1.0	9.8	3.36	9.14	0.45	0.45
n = 21	Mean	19.9	2.7	2.4	1.7	14,315	262.8	–	7598.0	5.1	78.4	193.5	750.8	7.6	28.7	18.4	12.3	1.4	40.40
	s.d	35.1	1.4	2.9	1.3	9317	198.2	–	3004.1	5.0	107.5	126.1	850.9	4.8	18.5	12.21	3.42	0.99	72.91
MVT deposit																			
	Max	–	2.1	–	12.3	77,235	302.0	0.8	26998.0	64.5	546.7	225.0	3493.0	75.4	11.0	1.40	1.17	43.60	6.22
	Min	–	0.1	–	0.1	985	1.0	0.01	956.0	0.7	2.15	1.0	28.0	3.5	0.3	0.10	0.16	0.06	0.01
n = 26	Mean	–	2.1	–	1.6	11,860	74.2	0.1	10303.2	11.5	82.39	28.6	473.7	11.1	4.2	0.57	0.51	4.08	0.83
	s.d	–	0.6	–	2.7	16,213	86.2	0.2	6306.6	15.3	117.04	59.0	803.1	15.7	3.7	0.48	0.25	9.30	1.95

Note: "-" means below the detection limit.

temperature sphalerite is conducive to the enrichment of Fe, Mn, Co and In, while high Cd, Ge, Ga and Tl contents are suggestive of low-temperature sphalerite (Ye et al., 2012; Wen et al., 2016a). At high temperatures, Se can enter the lattice of sphalerite instead of forming selenium minerals (Stillings, 2017). Sphalerite Co values are typically <5 ppm in all SEDEX and MVT deposits, but in the range of 18.0–282.0 ppm in the vein deposits. Sphalerite with high Co content is suggestive of skarn-type deposit, where its concentration can reach 2299 ppm (Cook et al., 2009; Ye et al., 2011). Also, sphalerite from vein deposits contain elevated levels of indium (Table 2, Figs. 6, 7), which is highly dispersed in the Earth's crust, with an average concentration of 0.05 ppm (Tu, 2002; Schwarz-Schampera and Herzig, 2002). The mineralization of In predominantly occurs in deposits related to magmatic-hydrothermal activities, and features in skarn, volcanic massive sulfide and epithermal deposit (Bauer et al., 2019; Dill et al., 2013; Schwarz-Schampera and Herzig, 2002; Sinclair et al., 2006; Werner et al., 2017; Li et al., 2020; Simons et al., 2017). Previous studies on C-H-O-Li-Pb-Cd-Zn isotopic variations in the vein type deposits considered in this study have shown that hydrothermal fluids arose from a magmatic hydrothermal system (Zhou et al., 2017; Xu et al., 2018; Zhou and Wen, 2021), as well.

SEDEX sphalerite have relatively higher Cr, V, Ge, As, and Ni contents. At the southeast margin of Yangtze block, episodic hydrothermal fluid exhalative events during the Neoproterozoic to early Cambrian had prompted the formation of unique Ni-Mo-PGE polymetallic sulfide-rich layers in the Niutitang Formation and V enriched shales in the Liuchapo formation (Fan et al., 2013; Fang et al., 2002; Jiang et al., 2006; Lott et al., 1999; Wen and Carignan, 2011). These characteristics indicate that Ni and V had accumulated in the deep anoxic zone of ocean. The abnormal geochemical background in this area may have great potential to provide sufficient Ni and V extracted into the SEDEX Zn-Pb hydrothermal solution.

The MVT sphalerites have relatively high Cd and Tl contents. Previous studies concluded that low temperature deposits have relatively high cadmium content (Schwartz, 2000; Wen et al., 2016a). This observation is consistent with analyses of the fluid inclusions in the MVT deposit which have shown that the temperature of the ore-forming fluid was in the range of 110–130 °C (Ye et al., 2018). The Cd (956.0–26998.0 ppm, average 10303.2 ± 6306.6 ppm) and Tl (0.06–43.6 ppm, average 4.08 ± 9.30 ppm) concentrations share a similar range to that of many MVT Pb-Zn deposits (Ye et al., 2011).

6.2. Sources of sulphur

Distinct sulphur isotope compositions have been recognized in sulphides (sphalerite, galena, pyrite and chalcopyrite) and/or sulphate (barite) selected from the vein type, SEDEX, and MVT deposits along the southeast margin of the Yangtze Block (Zhou et al., 2017, 2018; Fig. 8). Sulphide in vein type deposits show the lowest and narrowest range of $\delta^{34}S_{VCDT}$ values, in the range of 8.8‰ to 14.4‰. In contrast, sulphides in the SEDEX deposits have the broadest range of $\delta^{34}S$ values, from −17.4‰ to 30.0‰. Sulphides in the MVT deposits have the largest $\delta^{34}S$ values, in the range of 31.3‰–42.0‰ The $\delta^{34}S$ values of nonlinear curve fit (Gaussian) for sphalerite in these three types of deposits are centralized in 13.5‰, 13.9‰, and 32.8‰, respectively (Fig. 8). Barite selected from SEDEX deposits shows a broad range of $\delta^{34}S$ values, 29.5‰–48.3‰, much higher than the $\delta^{34}S$ values of sulphides in this type of deposit. By contrast, in the MVT deposits, barite have similar sulphur isotopic compositions to those of sulphides, in the range of 31.3‰–42.0‰.

Vein type deposits chiefly consist of sulphides without sulphate minerals, which suggests that the $\delta^{34}S$ value of sulphides can represent the sulphur isotopic compositions of the hydrothermal fluid ($\delta^{34}S_{\Sigma S} \approx \delta^{34}S_{sulfide}$). Compared with the SEDEX and MVT ores, the polymetallic veins show lower $\delta^{34}S_{VCDT}$ values. No organic matter was found in the ores, and no paleo-oil-field brines have been observed in the

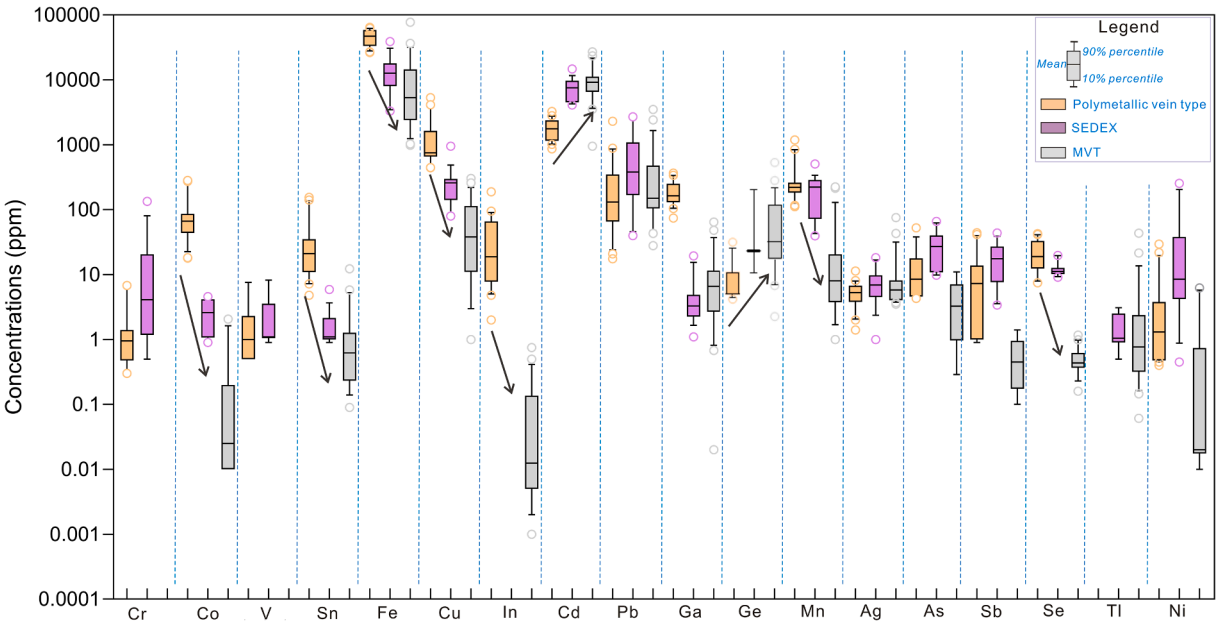

Fig. 6. Box and whisker plots showing trace elements of sphalerite from Zn-Pb deposits in the southeast margin of Yangtze Block.

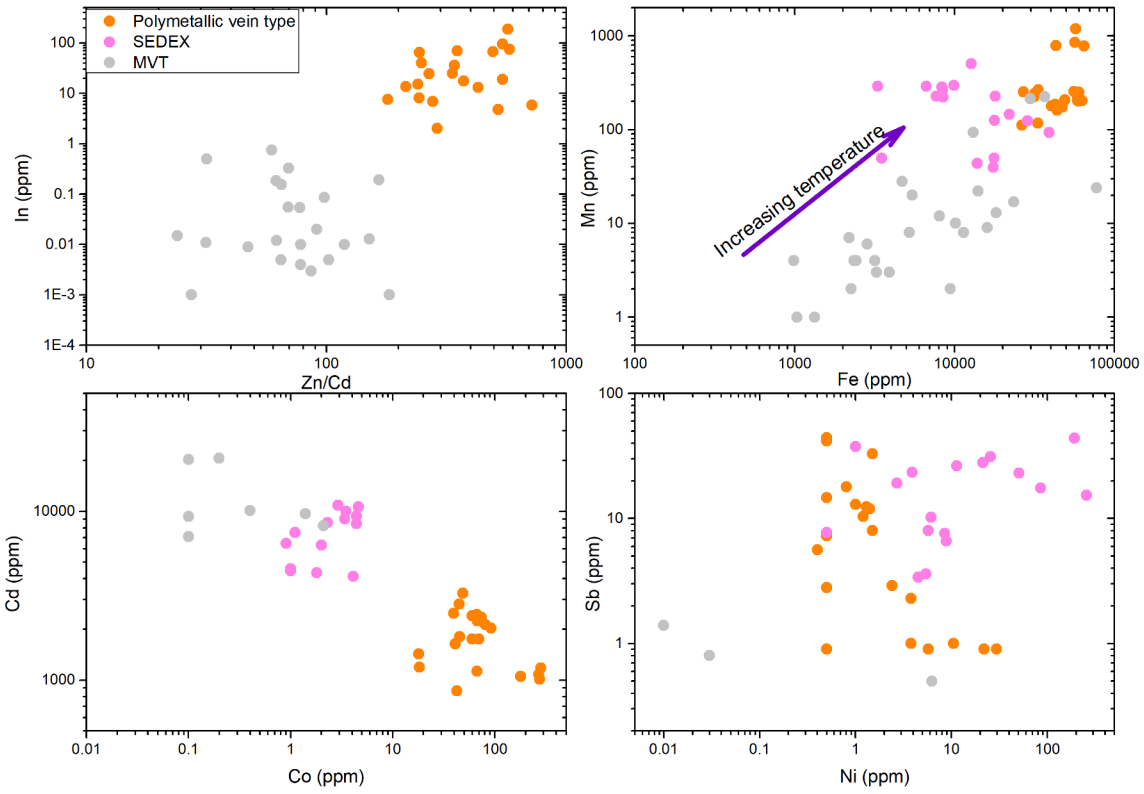

Fig. 7. Binary plots showing inter-element correlation in sphalerite. (a) Zn/Cd vs. In, (b) Fe vs. Mn, (c)Co vs. Cd, (d) Ni vs. Sb,

polymetallic vein orefields or nearby (Wang and Shi, 1997; Ye et al., 2012; Zhou et al., 2017; Cai et al., 2015). Moreover, marine evaporites and carbonates are scarce in the host rock. Therefore, the sulphur of polymetallic vein deposits is unlikely to have originated through bacterial sulphate reduction (BSR)/thermal sulphate reduction (TSR) processes of sulphate in the host rocks and contemporaneous seawater (Zhou et al., 2017). The homogeneous sulphur isotope composition suggests that the relatively high $\delta^{34}S$ values were inherited from ascending hydrothermal fluids (Zhou et al., 2017). Enrichment in ^{34}S relative to ordinary igneous rocks may be controlled by magmatic–hydrothermal fluids assimilating minerals with higher $\delta^{34}S$ values during upward movement (Leng et al., 2015), or may be the result of considerable degassing of SO_2 from the magma chamber (Zheng, 1990).

Based on a comparison with the marine sulphate composition and mean sedimentary pyrite composition produced by BSR reported by Farquhar et al. (2010), we can recognize that sulphur of the SEDEX and MVT deposits was sourced from early Cambrian seawater and contemporaneous connate water trapped in the surrounding rocks, respectively

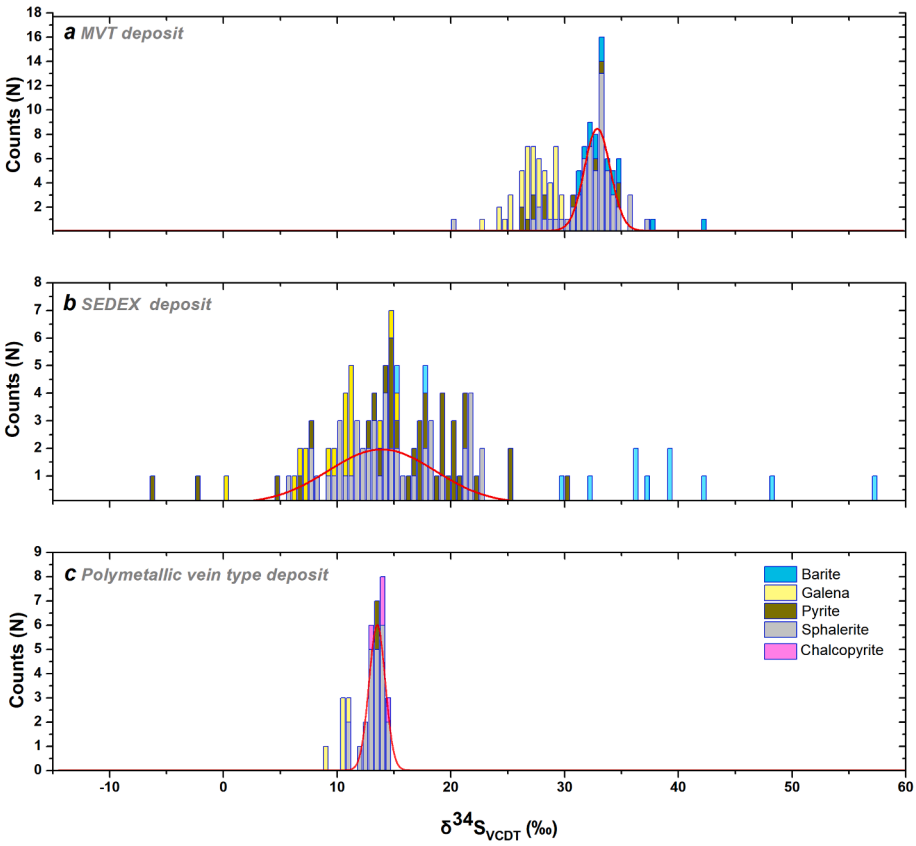

Fig. 8. Histograms of $\delta^{34}S_{VCDT}$ of sulphide and sulphate minerals from the southeast margin of Yangtze Block.

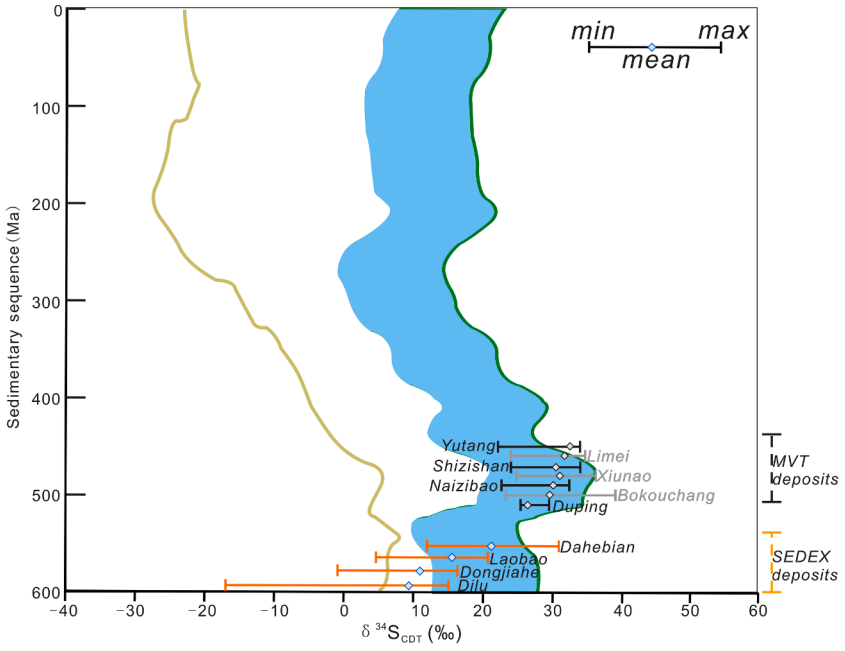

Fig. 9. Diagram illustrating range and median $\delta^{34}S$ values of sulphides in a selection of SEDEX and MVT deposits plotted at their approximate host-rock/formation age compared with marine sulphate composition (green line) and mean sedimentary pyrite composition (olive line) as produced by BSR. Data of green line and olive line were compiled in Kiyosu and Krouse, 1990, Farquhar et al., 2010, and Wilkinson, 2014. (For interpretation of the references to colour in this figure legend, the reader is referred to the web version of this article.)

(Fig. 9).

(1) SEDEX Ores: Sulphides in the recharge zone of the SEDEX system and stratiform barite layers have similar sulphur isotopic compositions. Additionally, barite selected from the recharge zone and the stratiform barite ore have similar sulphur isotopic compositions (Table 3 and Fig. 8). Zhou et al. (2018) calculated the sulphur isotopic fractionation between minerals (barite and sulphide) and the early Cambrian seawater: $\Delta^{34}S_{Barite\text{-}Seawater} = 7.8‰$ and $\Delta^{34}S_{Sulphide\text{-}Seawater} = -12.1‰$, respectively.

The $\delta^{34}S$ values of sulphides in the SEDEX ores are mostly consistent with the field of TSR of early Cambrian seawater sulphate (Fig. 9). The Dahebian Pb–Zn deposit is located in the slope facies of the Nanhua Basin, which is rich in organic matter. We observed bitumen and sulphide intergrowth in drill core samples from the Dahebian and

Table 3
Sulfur isotope of sulfide minerals and barite from the southeast margin of Yangtze Block.

Minerals	Counts	δ34S (‰)			
		Max	Min	Mean	s.d
Polymetallic vein deposits					
Sphalerite	23	14.4	10.7	12.9	0.96
Pyrite	2	13.4	13	13.2	0.28
Galena	5	10.3	8.8	10	0.69
Chalcopyrite	4	14.2	12.9	13.7	0.56
SEDEX deposits					
Sphalerite	46	22.9	5.6	14.6	4.50
Pyrite	36	30	−6.1	16.2	7.06
Galena	18	15	−17.4	8.4	7.31
Barite	12	57.4	15.4	35.9	11.63
MVT deposits					
Sphalerite	66	37.2	20.3	32.3	2.46
Pyrite	12	34.7	26.3	29.7	3.40
Galena	37	29.7	22.8	27.2	1.76
Barite	16	42	31.1	33.8	2.70

Table 4
Lead isotope of sulfide minerals and sedimentary sequence from the southeast margin of Yangtze Block.

	$^{206}Pb/^{204}Pb$	$^{207}Pb/^{204}Pb$	$^{208}Pb/^{204}Pb$
Polymatellic vein deposit n = 12			
Max	17.258	15.508	37.546
Min	17.139	15.432	37.282
Mean	17.189	15.461	37.381
s.d.	0.029	0.021	0.086
SEDEX deposit n = 23			
Max	17.750	15.586	37.801
Min	17.597	15.537	37.587
Mean	17.702	15.574	37.717
s.d.	0.032	0.011	0.041
MVT deposit n = 50			
Max	18.266	15.875	38.888
Min	18.028	15.621	38.099
Mean	18.171	15.726	38.373
s.d.	0.051	0.049	0.156
Basement n = 37			
Max	22.038	15.937	46.917
Min	17.507	15.430	37.876
Mean	18.501	15.600	39.514
s.d.	1.047	0.116	1.816
Liuchapo Fm. n = 4			
Max	18.484	15.686	38.343
Min	17.559	15.636	37.919
Mean	17.937	15.659	38.137
s.d.	0.426	0.021	0.179
Niutitang Fm. n = 15			
Max	18.817	15.721	38.619
Min	16.345	15.486	37.369
Mean	17.932	15.651	37.990
s.d.	0.624	0.063	0.307
Qinxudong Fm. n = 10			
Max	19.073	15.783	39.408
Min	18.067	15.626	38.107
Mean	18.464	15.701	38.532
s.d.	0.404	0.058	0.398

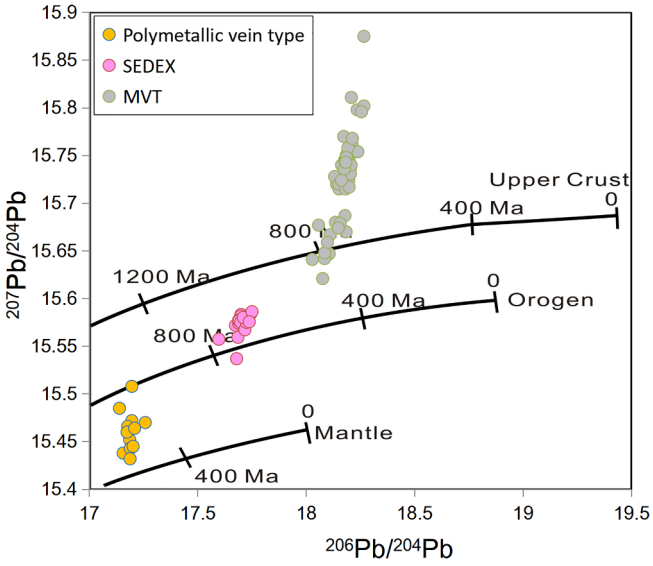

Fig. 10. Plots of $^{206}Pb/^{204}Pb$ vs. $^{207}Pb/^{204}Pb$ for sulphide minerals from the southeast margin of Yangtze Block.

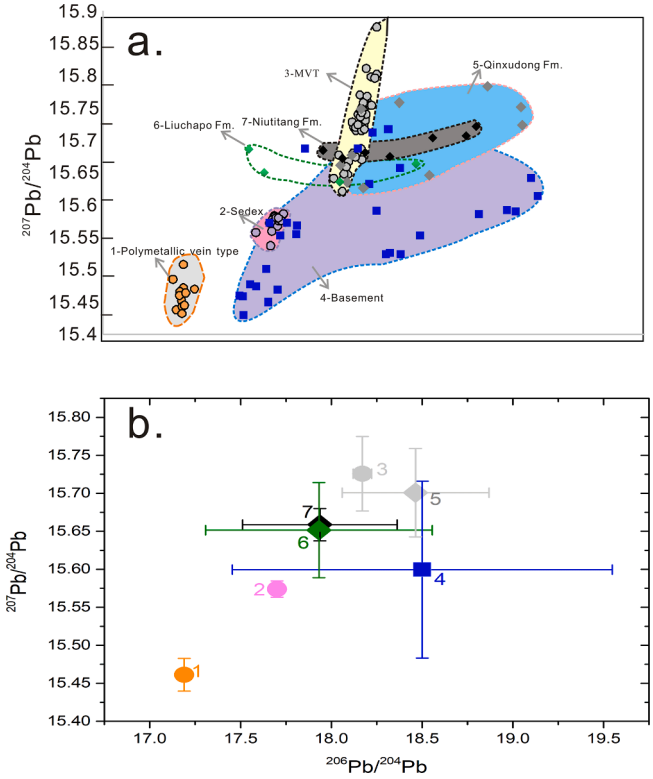

Fig. 11. (a) Plots of $^{206}Pb/^{204}Pb$ vs. $^{207}Pb/^{204}Pb$ for sulphide minerals and sedimentary sequence from the southeast margin of the Yangtze Block; (b) Plots of the mean values of $^{206}Pb/^{204}Pb$ vs. $^{207}Pb/^{204}Pb$ of different units.

Dongjiahe deposits (Fig. 5f). Under the microscope, sphalerite and pyrite particles displayed mosaic pattern in bitumen (Zhou et al., 2018). The pyrite in the main ore-forming stage was mainly fine-grained, representing rapid crystallization with a rapid H_2S generation rate of sulphate reduction. Fluid inclusions captured by sphalerite, barite, and quartz in the Dahebian Pb–Zn deposit recorded high homogenization temperatures (up to 352 °C; Wen et al., 2017; Zhou et al., 2018). Thus, all these phenomena indicate that TSR occurred during Pb–Zn mineralization

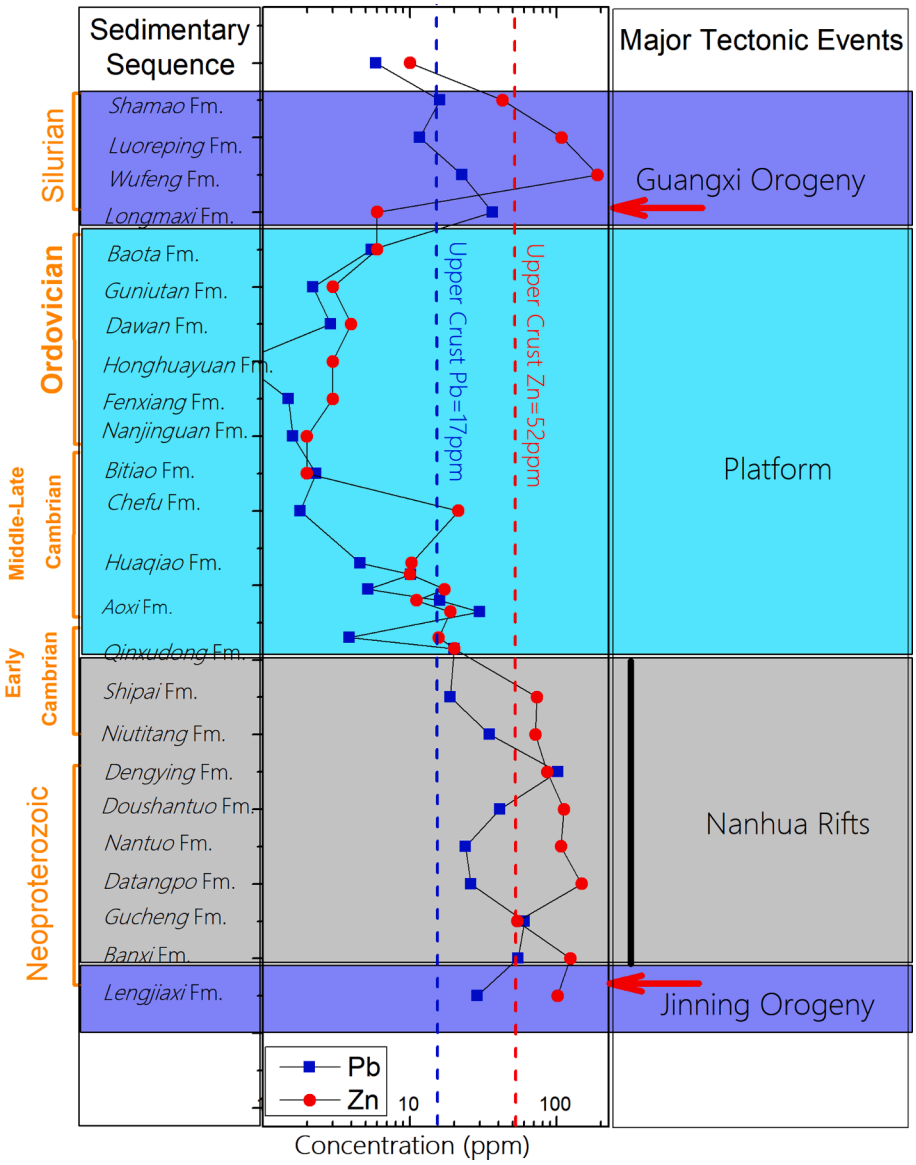

Fig. 12. Zinc and lead concentrations of sedimentary sequence from the southeast margin of the Yangtze Block.

(Machel et al., 1995), and demonstrate that the sulphur in the SEDEX ores was derived from the early Cambrian stratified seawater column.

However, in some local cases, such as the Dilu, Dongjiahe and Laobao deposits, $\delta^{34}S$ values were lower than those in the Dahebian region, almost consistent with the $\delta^{34}S$ value line of mean sedimentary pyrite composition as produced by BSR. Galena from the Dilu deposit yielded a $\delta^{34}S$ value as low as −17.4‰ (Fig. 9; Luo et al., 1990). The fractionation of sulphur isotopes of this galena and early Cambrian sulphate is about −49‰. Such broad sulphur isotope fractionation is caused in natural environments by BSR (Ohmoto, 1972; Machel et al., 1995). Compared with the Dahebian Pb–Zn deposits, the Dongjiahe, Dilu, and Laobao Pb–Zn deposits were located closer to the basin area and in deeper water settings (Luo, 1990; Zeng and Li, 2007; Liang et al., 2009; Liao et al., 2013; Xiang and Luo, 2013; Wen et al., 2017). The organic matter content in slope to basinal sediments was higher, corresponding to more extensive BSR processes.

(2) MVT ores: The mineralization fluids of MVT deposits tend to be oxidized, and barite from the upper part of the Niutitang Formation may have been difficult to remove in oxidizing fluids (Cooke et al., 2000). Thus, bedded barite ore providing large amounts of sulphur to the MVT deposits in this region (Duan, 2014; Zhou, 2017) is debatable. These MVT Pb–Zn deposits have similar sulfur isotopic compositions to that of the early Cambrian seawater ($\delta^{34}S_{VCDT}$ = 27‰–32‰; Fig. 9; Farquhar et al., 2010). Sulphur from Pb–Zn deposits hosted by sedimentary rocks is mainly provided by the sulphate reduction of gypsum salts and connate water trapped in the surrounding rock. The mineralization temperature of this type of Pb–Zn deposit is within 150–200°C, which is higher than the upper limit of survival for sulphate-reducing bacteria. Therefore, sulphur was likely mainly provided by TSR. Liu and Zheng (2000) studied the surrounding rock, the compositions of gas and liquid in inclusions, the organic geochemistry, as well as the C, O and S isotopes in the Huayuan mining area finding that a large amount of sulphur was provided by TSR. Sulphur isotopic fractionation between sulphide and early Cambrian sulphate was within 10‰, indicating relatively rapid sulphate reduction.

6.3. Sources of metal

The zinc and lead concentrations of the Neoproterozoic to middle Cambrian sedimentary strata in the south-eastern Yangtze Block are higher than their concentrations in the upper crust (Fig. 12; Zn: 52 ppm, Pb: 17 ppm; Wedepohl, 1995; Zhang et al., 2013a; Duan, 2014).

Sediments deposited from the late middle Cambrian to the Ordovician, in contrast, are below the abundance of Zn-Pb in the upper crust. During the episodic rifting of the Nanhua Basin, the seawater was characterized by long-term stratification and widespread water-column anoxia (Li et al., 2010, 2012, 2015; Feng et al., 2010; Fan et al., 2013; Wen et al., 2016a). The deep seawater was mainly anoxic, as indicated by the deposition of thick reduced sediments. Ba^{2+}, Fe^{2+}, and Zn^{2+}, carried by exhalative hydrothermal fluids and weathered continental materials (Shields, 2005; Fan et al., 2013; Huang et al., 2011; Zhou et al., 2010), facilitated their accumulation in the reduced sediments (Zhou et al., 2018). In particular, the Datangpo, Liuchapo and Niutitang formations, which are rich in organic matter and formed in stratified seawater settings, were relatively enriched in Zn–Pb (Fig. 12a-2).Sulfur isotopes of both MVT and SEDEX deposits reflect an early Cambrian seawater source, either directly from seawater or connate water, thus indicating that early Cambrian sediments might play an important role in providing lead and other metals for mineralization.

Similar to the sulfur isotopes, the lead isotopic variations in the vein type, SEDEX and MVT deposits differed from each other. In the diagram of $^{206}Pb/^{204}Pb$ versus $^{207}Pb/^{204}Pb$, each type has its own distinct field (Fig. 9). Sulphides from the vein type deposits have the lowest and most homogeneous radiogenic lead isotopic values in the south-eastern Yangtze Block. On the contrary, sulphides collected from the MVT deposits have the highest radiogenic lead isotope values and showed a positive correlation between $^{206}Pb/^{204}Pb$ and $^{207}Pb/^{204}Pb$ values. Sulphides selected from the vein type, SEDEX, and MVT deposits plot between the orogenic and mantle lead curves, between the upper crust and orogenic lead curves, and close to or above the upper crust lead evolution curves (Zartman and Doe, 1981), respectively (Fig. 10). Therefore, the ore-forming metals of the vein type deposits were mostly sourced from a mixed-mantle source and a crustal source (Zhou et al., 2017), whereas the metals of the SEDEX and MVT deposits were likely derived from the upper crust (Zhou et al., 2018, and references therein). In comparison with lead isotopic variations of basement rock and sedimentary rocks (Fig. 11), the following characteristics could be recognized:

Lead isotopic compositions of samples from the vein type deposits are homogeneous and show a distinctly different signature from the basement rocks and early Cambrian sedimentary rocks. This suggests that the basement rocks and early Cambrian sediments provided very little, if any, metals to these vein type ores (Zhou et al., 2017). As mentioned above, the vein type deposits have shown that mineralizing fluids belonged to a high temperature magmatism-related hydrothermal system. A deeply concealed pluton might have provided ore-forming metals for vein-type mineralization.

Similar Pb isotopic signatures between the SEDEX deposits and the basement rocks support that hydrothermal fluids circulated in basement rocks and scavenged Zn–Pb into the ore-forming fluids. The basement source of metals was similar to other SEDEX Zn-Pb deposits, suggesting that metals are sourced from clastic-dominated sedimentary rock sequences and basement rock (Wilkinson, 2014).

Lead isotopic compositions of MVT deposits have a positive correlation on both $^{207}Pb/^{204}Pb$ versus $^{206}Pb/^{204}Pb$ and $^{208}Pb/^{204}Pb$ versus $^{206}Pb/^{204}Pb$. Previous studies explained the collinear trends by the mixing of two or more endmembers fluids at deposition site (Schneider et al., 2002; Ayuso et al., 2004) or differential leaching and extraction of metals from an independent homogeneous source (Field et al., 2018). In consideration of Pb isotopic values mostly falling outside of the field for basement rocks (the possible independent homogeneous source at our study region), it figures that an independent homogeneous source is unlikely to result in the observed collinear trends. Thus, the mixing of two or more fluids with distinct lead isotopic compositions is more plausible. Samples from the MVT deposits mostly overlapped with the field of the early Cambrian sediments (Fig. 11; Liuchapo formation, Niutitang formation, and Qinxudong formation), and less importantly, the basement rocks. We infer that mineralizing metals were chiefly derived from the early Cambrian sediments, but mixing with fluids which had scavenged metals from basement rocks.

6.4. Implications for ore genesis

(1) *Genetic model for SEDEX ores:*

The SEDEX deposits formed during the early Cambrian (Zhou et al., 2018). Based on zircon SHRIMP U–Pb ages from a potassium bentonite layer in the upper Laobao Formation (536 ± 5 Ma; Zhou et al., 2013a,b) and the Re–Os ages of a Ni–Mo–PGE layer in the lower Niutitang Formation (521 ± 5 Ma; Xu et al., 2011), we can constrain the formation of the inter-layer barite ores to 541–516 Ma. The SEDEX Pb–Zn deposits, which mainly formed in the recharge zone of these exhalative fluids, occurred in this period.

During the late Ediacaran to early Cambrian, the sedimentary facies of the southeast margin of the Yangtze Block evolved from open shelf to rimmed shelf (Fig. 12a-1; Condon et al., 2005; Jiang et al., 2006; Zhou et al., 2018). Intensive fault depressions and extensions in the Nanhua Basin resulted in high geothermal gradients (Fang et al., 2002). Seawater from evaporative environments on the rimmed shelf infiltrated along extensional faults in thick reduced Neoproterozoic sediments and scavenged metals, eventually evolving into acidic, reducing and metalliferous hydrothermal fluids (Fig. 12a-2). When hydrothermal fluids migrated into the *syn*-sedimentary faults beneath the basin, they ascended along these faults. In the recharge zone of the hydrothermal systems, sulphide mineralization was mainly triggered by mixing of upward metallififerous fluids and H_2S-enrich bottom seawater. In the southeast margin of Yangtze Block, the Doushantuo Formation was characterized by the development of sheet cracks and small stacked or karstic dissolution cavities, which were conceivably caused by repeated transgression-regression episodes, postglacial isostatic rebound, and methane release effects during the early Ediacaran (Hoffman and Macdonald, 2010; Jiang et al., 2006; Meyer and Kump, 2008; Zhou et al., 2010). These might be the principal reasons that the "recharge zone mineralization" was primarily situated in the Doushantuo Formation. Ultimately, the hydrothermal fluids vented into the seafloor and continuous mixing with the progressively oxidizing seawater resulted in rapid precipitation of barite as stratiform ore on the seafloor (Feng et al., 2010; Holland and Malinin, 1979; Jiang et al., 2011; Johnson et al., 2004; Wen et al., 2016a,b), as well as voluminous *syn*-depositional fine-grained sphalerite and pyrite in the stratiform barites ores.

(2) *Genetic model for MVT ores:*

The MVT Zn–Pb deposits formed in the interval from 480 Ma to 410 Ma (Ye et al., 2012; Duan et al., 2014; Zhou et al., 2014). This period was contemporary with the primary episode of the Guangxi Orogeny (ca. 462 Ma to 396 Ma; Fig. 11b-1; Chen et al., 2010, 2012; Hu et al., 2010; Wang et al., 2012). Accordingly, the Guangxi orogeny caused the formation of foreland basin along the southeast margin of Yangtze Block (Jin, 2010; Wang et al., 2011; Zhou et al., 2018). MVT deposits in the study region were located at these foreland basins and the mineralization was occurred in platform carbonate sequences. It is generally accepted that MVT deposits were produced by enormous amounts of brines that migrated through foreland basins (Bradley and Leach, 2003). Therefore, in its tectonic aspects, MVT Zn–Pb mineralization at the southeast margin of the Yangtze Block was mainly controlled by the Guangxi Orogeny.

The Xintao and Xiaoheba intervals of the Silurian were major development stages of the foreland basins (Li et al., 2015a,b, 2016). These foreland basins evolved from sedimentary sequences of clastic sediments in continental rifts and passive continental margin settings

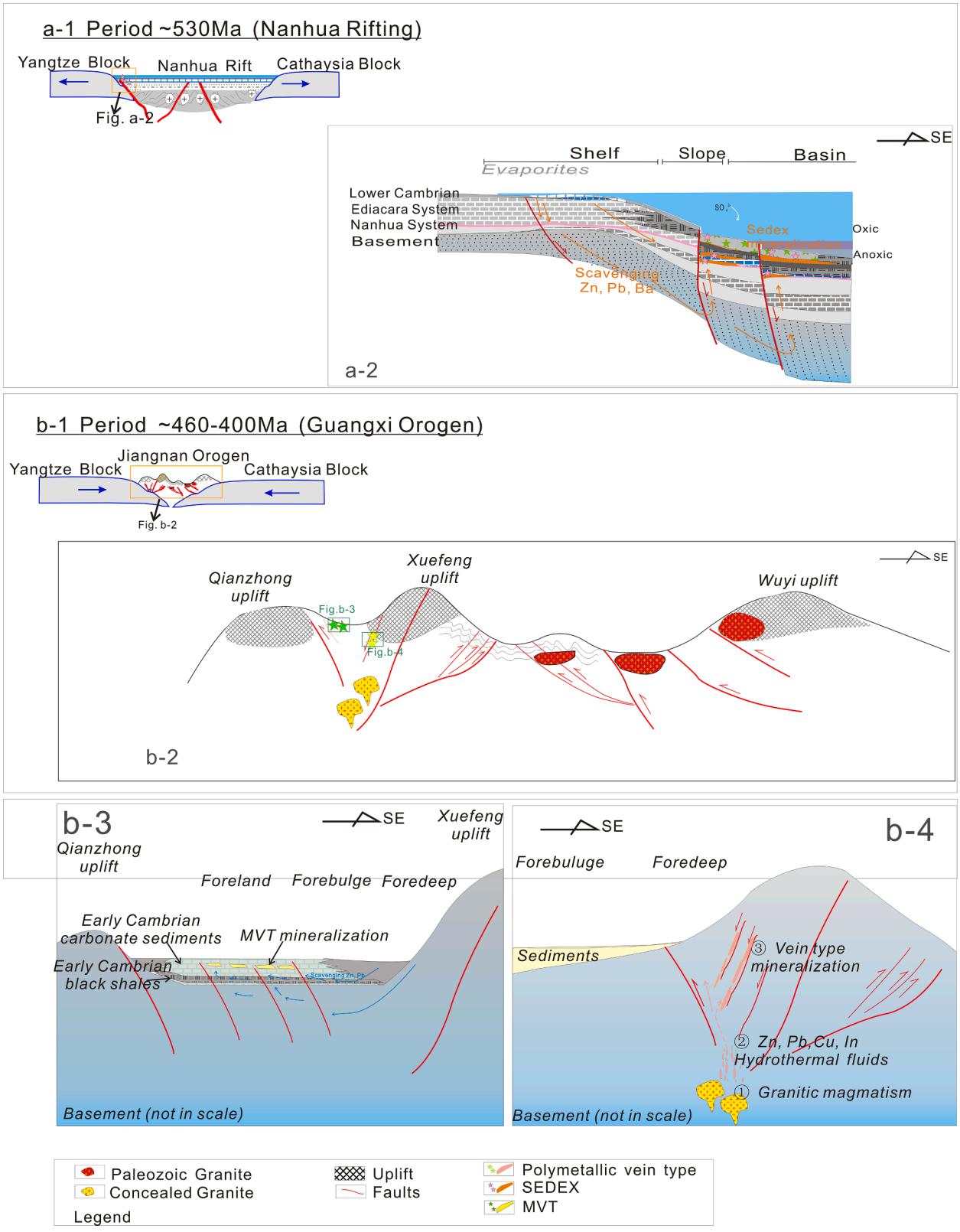

Fig. 13. Schematic diagram illustrating the genetic model of Zn-Pb deposit along the southeast margin of the Yangtze Block. (a-1) Paleotectonic setting during the SEDEX mineralization at the southeast margin of the Yangtze Block; (a-2) Genetic model for the SEDEX deposits in a rift basin setting during the Nanhua rifting activity (modified from Zhou et al., 2018); (b-1) Paleotectonic setting during the Guangxi orogeny at the southeast margin of the Yangtze Block; (b-2) Schematic diagram of thrust system of the Guangxi Orogen (modified from Jin, 2010); (b-3) Genetic model for the MVT deposits and (b-4) polymetallic vein deposits in the foreland basin setting.

from the Neoproterozoic onward. Hydrothermal fluids were expelled by the intracontinental orogeny between the Cathaysia Block and the Yangtze Block. Fluids ascended through basement rocks and into the early Cambrian sediments of the foreland basin and scavenged metals. At the blocking effect of the Qianzhong uplift to the west, basinal brines were likely gathering from the Chadong–Huayuan–Zhangjiajie fault to the Baojing–Tongren–Yuping fault (Fig. 12b-3; Jin, 2010; Li et al., 2015a,b, 2016). Sulfide deposited triggered by the mixing of metalliferous fluids and the H_2S-rich fluid originated from connate water within surrounding sediments.

(3) *Genetic model for polymetallic vein ores:*

Polymetallic vein-type Zn-Pb deposits are fault-bounded in upper part of the Banxi Group. Since the deposition of Banxi Group, the southeast margin of the Yangtze Block mainly evolved as a passive continental margin, then turned into a foreland basin under the effect of the Guangxi Orogeny. After that, the southeast margin of the Yangtze Block was relatively "quite" and only suffered from mild structural deformation at the shallow crust scale. The Guangxi Orogeny was a critical tectonic-thermal event in the southeastern Yangtze Block, and promoted regional MVT Zn–Pb mineralization, quartz vein-type Au mineralization and vein-type W–Cu mineralization. Hence, it is plausible that the mineralizing fluids may be sourced from magmatic differentiation or metamorphic devolatilization in the period of the Guangxi Orogeny. Pb isotopic values of sulphides point out the ore-forming metals of the vein-type deposits were mostly sourced from a mixed mantle and crust source. Robust isotopic evidences (Zn–Cd isotopic variations of sphalerite (Zhou and Wen, 2021); C–O isotopic variations of carbonate minerals (Zhou et al., 2017); H–O–Li isotopic variations of fluid inclusions (Xu et al., 2018; Zhou et al., 2017) indicates that they are invariably magmatic–hydrothermal origin.

A challenge to the magmatic–hydrothermal model might be the lack of pluton outcrops around the polymetallic vein ore fields. However, various dome-shaped structures and residual gravity anomalies suggest the presence of magmatic plutons at depth in vein type mineralization area (Peng et al., 2003; Wan, 1986; Wang et al., 2011; Yang et al., 2015; Zhou et al., 2017). Regionally, to the south, apart from the ore field of about 100 km, there are voluminous ca. 464–400 Ma, high-K calc-alkaline series peraluminous granitoids (with ages peaking at ca. 446–420 Ma; such as Baimashan and Miao'ershan plutons; Bai et al., 2015). This period of granitic magma promoted extensive W–Cu mineralization, such as the Dushiling W–Cu deposit (417 ± 35 Ma; Chen et al., 2016) and the Luchongping deposit (437–390 Ma; Zhang et al., 2017). Indium and Sn bearing polymetallic hydrothermal fluids are often associated with granitic magma differentiation (Sinclair et al., 2006; Simons et al., 2017). Thus, we propose that the vein-type mineralization was triggered by granitic magma within the Guangxi Orogeny. There Zn, Cd, Cu, In and Sn-bearing hydrothermal fluids are derived from the fractionation of granitic magma and, after ascending along faults, eventually triggered polymetallic vein-type mineralization at suitable zones in upper part of the Banxi Group (Fig. 13b-4).

7. Concluding remarks

The southeastern margin of the Yangtze Block mainly comprises polymetallic vein-type, SEDEX and MVT Zn–Pb deposits. Sphalerite in the polymetallic vein-type deposits is rich in Fe, In, Co, Ga, and Cu, whereas sphalerite in the SEDEX deposits and MVT deposits is rich in Cd and Ge, but depleted in Fe, In, and Ga.

Sulphur of the vein-type mineralization was derived from magmatic–hydrothermal sources. Sulphur in the SEDEX ore was derived from early Cambrian stratified seawater sulfate through TSR and BSR processes, whereas sulphur in the MVT ores was mainly provided by TSR of sulfate in connate water.

The primary suppliers of metals were different for the three types of mineralization considered at the southeastern margin of the Yangtze Block. The granitic magmatism related to the Guangxi Orogeny was essential for the vein type deposits. Basement rocks provided metals for the SEDEX deposits, whereas early Cambrian sediments together with basements rocks might have been the metal sources of the MVT mineralization.

The Nanhua rifting lead to the formation of the syngenetic Zn-Pb mineralization, while the Guangxi Orogeny controlled the mineralization of the magmatic-hydrothermal vein deposits at depth part and the MVT mineralization at shallower crustal levels.

Declaration of Competing Interest

The authors declare that they have no known competing financial interests or personal relationships that could have appeared to influence the work reported in this paper.

Acknowledgements

This project was financially co-supported by the National Natural Science Foundation of China (Grant No. 41903037), the National Key R&D Program of China (Grant No. 2017YFC0602500), the Jiangxi Provincial Natural Science Foundation (Grant No. 20212BAB213010), the discretionary foundation of the State Key Laboratory of Nuclear Resources and Environment (Grant No. Z1915) and the foundations of Doctor of East China University of Technology (Grant No. DHBK2018036). We are grateful to associate Editor Dr. Marilena Moroni and two anonymous reviewers for their constructive and helpful comments to improve this paper.

Appendix A. Supplementary data

Supplementary data to this article can be found online at https://doi.org/10.1016/j.oregeorev.2022.104957.

References

Ayuso, R.A., Kelley, K.D., Leach, D.L., Young, L.E., Wandless, J.F.S., Lyon, A.M., Dillingham, J.L., 2004. Origin of the Red Dog Pb-Zn-Ag deposits, Brooks Range, Alaska: Evidence from regional Pb and Sr isotope sources. Econ. Geol. 99 (7), 1533–1553.

Bai, D.Y., Zhong, X., Jia, P.Y., Xiong, X., Huang, W.Y., 2015. The zircon SHRIMP U-Pb dating, geochemical characteristics and tectonic setting of Caledonian Yuechengling pluton in the western segment of the Nanling Mountains. Geochimica 44 (1), 27–42 (in Chinese with English abstract).

Bauer, M., Seifert, T., Burisch, M., et al., 2019. Indium-bearing sulfides from the Hämmerlein skarn deposit, Erzgebirge, Germany: evidence for late-stage diffusion of indium into sphalerite. Miner. Deposita 54, 175–192.

Bradley, D.C., Leach, D.L., 2003. Tectonic controls of Mississippi Valley-type lead–zinc mineralization in orogenic forelands. Miner. Deposita 38, 652–667.

Cai, C.F., Worden, R.H., Bottrell, S.H., Wang, L.S., Yang, C.C., 2003. Thermochemical sulphate reduction and the generation of hydrogen sulphide and thiols (mercaptans) in Triassic carbonate reservoirs from the Sichuan Basin, China. Chem. Geol. 202 (1), 39–57.

Cai, C., Xiang, L., Yuan, Y., He, X., Chu, X., Chen, Y., 2015. Marine C, S and N biogeochemical processes in the redox-stratified early Cambrian Yangtze ocean. Journal of the Geological Society 172 (3), 895–903 (in Chinese with English abstract).

Chang, Z., Shu, Q., Meinert, L.D., 2019. Skarn deposits of China. Society of Economic Geologists, Special Publication 22, 189–234.

Charvet, J., Shu, L., Faure, M., Choulet, F., Wang, B., Lu, H., Breton, N.L., 2010. Structural development of the lower paleozoic belt of South China: genesis of an intracontinental orogen. J. Asian Earth Sci. 39 (4), 309–330.

Chen, X., Zhang, Y.D., Fan, J.X., Cheng, J.F., Li, Q.J., 2010. Ordovician graptolite-bearing strata in southern Jiangxi with a special reference to the Kwangsian orogeny. Sci. China Earth Sci. 53 (11), 1602–1610.

Chen, W.D., Zhang, W.L., Wang, R.C., Chu, Z.Y., Xiao, R., Zhang, D., Che, X.D., 2016. A study on the Dushiling tungsten-copper deposit in the Miao'ershan-Yuechengling area, Northern Guangxi, China: implications for variations in the mineralization of multi-aged composite granite plutons. Sci. China Earth Sci. 59 (11), 2121–2141.

Chen, X., Zhang, Y.G., Fan, J.X., Tang, L., Sun, H.Q., 2012. Onset of the Kwangsian Orogeny as evidenced by biofacies and lithofacies. Sci. China Earth Sci. 55, 1592–1600. https://doi.org/10.1007/s11430-012-4490-4.

Condon, D., Zhu, M., Bowring, S., Wang, W., Yang, A., Jin, Y., 2005. U-Pb ages from the Neoproterozoic Doushantuo Formation, China. Science 308 (5718), 95–98.
Cook, N.J., Ciobanu, C.L., Pring, A., Skinner, W., Shimizu, M., Danyushevsky, L., Saini-Eidukat, B., Melcher, F., 2009. Trace and minor elements in sphalerite: A LA-ICPMS study. Geochim. Cosmochim. Acta 73, 4761–4791. https://doi.org/10.1016/j.gca.2009.05.045.
Cooke, DR, Bull, SW, Large, RR, Mcgoldrick, PJ, 2000. The importance of oxidized brines for the formation of Australian Proterozoic stratiform sediment-hosted Pb-Zn (Sedex) deposits. Economic Geology 95 (1), 1–18.
Cugerone, A., Cenko-Tok, B., Oliot, E., Munoz, M., Barou, F., Motto-Ros, V., Le Goff, E., 2019. Redistribution of germanium during dynamic recrystallization of sphalerite. Geology 48. https://doi.org/10.1130/G46791.1.
Dill, H.G., Garrido, M.M., Melcher, F., Gomez, M.C., Weber, B., Luna, L.I., Bahr, A., 2013. Sulfidic and non-sulfidic indium mineralization of the epithermal Au–Cu–Zn–Pb–Ag deposit Aan Roque (Provincia Rio Negro, SE Argentina) -with special reference to the "indium window" in zinc sulfide. Ore Geol. Rev. 51, 103–128.
Du, S.J., Wen, H.J., Zhu, C.W., Luo, C.G., Zhou, Z.B., Yang, Z.M., Chen, J.S., Zhu, X., 2019. Geochemical background on the super-richening of disperse metal elements on the western margin of the Yangtze plate. Acta Petrol. Sin. 35 (11), 3355–3369. https://doi.org/10.18654/1000-0569/2019.11.06 (in Chinese with English Abstract).
Duan, Q.F., 2014. The Research of the Metallogenic Regularity of Stratabound Zinc-Lead Deposits from Sinian-Cambrian in the Western Hunan and Eestern Hubei. Doctor thesis of. China University of Geosciences, Wuhan.
Duan, Q.F., Gao, L., Zeng, J.K., Zhou, Y., Tang, Z.Y., Li, K., 2014. Rb-Sr dating of sphalerite from Shizishan Pb-Zn deposit in Huayuan ore concentration area, westerm Hunan, and its geological significance. Earth Sci.-J. China Univ. Geosci. 39 (8), 977–999 (in Chinese with English abstract).
EU Commission, 2014. Critical raw materials for the EU. Report of the Ad hoc Working Group on Defining Critical Raw Materials, Brussels.
Fan, H., Wen, H., Zhu, X., Hu, R., Tian, S., 2013. Hydrothermal activity during Ediacaran-Cambrian transition: silicon isotopic evidence. Precambr. Res. 224 (224), 23–35.
Fang, W.X., Hu, R.Z., Su, W.C., Qi, L., Xiao, J.F., Jiang, G.H., 2002. Geochemical characteristics of Dahebian-Gongxi superlarge barite deposits and analysis on its background of tectonic geology, China. Acta Petrol. Sin. 18 (2), 247–256 (in Chinese with English abstract).
Farquhar, J., Wu, N., Canfield, D.E., et al., 2010. Connections between sulfur cycle evolution, sulfur isotopes, sediments, and base metal sulfide deposits. Econ. Geol. 105 (3), 509–533.
Feng, L.J., Chu, X.L., Huang, J., Zhang, Q.R., Chang, H.J., 2010. Reconstruction of paleo-redox conditions and early sulfur cycling during deposition of the Cryogenian Datangpo Formation in South China. Gondwana Res. 18 (4), 632–637.
Field, J.D., Appold, M.S., Renson, V., Coveney, R.M., 2018. Lead and sulfur isotope composition of trace occurrences of Mississippi Valley-type mineralization in the U. S. midcontinent. J. Geochem. Explor. 184, 66–81.
Frenzel, M., Hirsch, T., Gutzmer, J., 2016a. Gallium, germanium, indium, and other trace and minor elements in sphalerite as a function of deposit type — A meta-analysis. Ore Geol. Rev. 76, 52–78.
Frenzel, M., Voudouris, P., Cook, N.J., Ciobanu, C.L., Gilbert, S., Wade, B.P., 2016b. Evolution of a hydrothermal ore-forming system recorded by sulfde mineral chemistry: a case study from the Plaka Pb–Zn–Ag Deposit, Lavrion, Greece. Mineral. Deposita. https://doi.org/10.1007/s00126-021-01067-y.
Frenzel, M, Voudouris, P, Cook, NJ, Ciobanu, CL, Gilbert, S, Wade, BP, 2022. Evolution of a hydrothermal ore-forming system recorded by sulfde mineral chemistry: a case study from the Plaka Pb–Zn–Ag Deposit, Lavrion, Greece. Mineralium Deposita 57, 417–438.
Gagnevin, G., Menuge, J.F., Kronz, A., Barrie, C., Boyce, A.J., 2014. Minor elements in layered sphalerite as a record of fluid origin, mixing, and crystallization in the Navan Zn-Pb Ore Deposit, Ireland. Econ. Geol. 109, 1513–1528.
Goodfellow, W.D., Jonasson, I.R., 1984. Ocean stagnation and ventilation defined by δ34S secular trends in pyrite and barite, Selwyn basin. Yukon Geol. 12 (10), 583–586.
Hoffman, P.F., Macdonald, F.A., 2010. Sheet-crack cements and early regression in Marinoan (635 Ma) cap dolostones: regional benchmarks of vanishing ice-sheets? Earth Planetary Science Letters 300 (3–4), 374–384.
Hoggard, M.J., Czarnota, K., Richards, F.D., Huston, D.L., Ghelichkhan, S., 2020. Global distribution of sediment-hosted metals controlled by craton edge stability. Nat. Geosci. 13 (7), 504–510.
Holland, H.D., Malinin, S.D., 1979. The solubility and occurrence of non-ore minerals. In: Barnes, H.L. (Ed.), Geochemistry of Hydrothermal Ore Deposits. John Wiley, New York, pp. 461–508.
Hu, S.Q., Zhu, G., Zhang, B.L., Zhang, L., 2010. K-Ar geochronology of the Caledonian event in the Xufeng uplift. Geol. Rev. 56 (4), 490–500 (in Chinese with English abstract).
Hu, T.P., Wang, M.F., Ding, Z.J., He, M.C., Wang, Y.B., Guo, X.N., 2017. C, O, S and Pb isotopic characteristics and sources of metallogenic materials of Limei Pb-Zn deposit in Huayuan County, western Hunan Province. Mineral Deposits 36 (3), 623–642 (in Chinese with English abstract).
Huang, J., Chu, X.L., Jiang, G.Q., Feng, L.J., Chang, H.J., 2011. Hydrothermal origin of elevated iron, manganese and redox-sensitive trace elements in the ca. 635 Ma Doushantuo cap carbonate. J. Geol. Soc. 168 (3), 805–816.
Jiang, G.Q., Kennedy, M.J., Christieblick, N., Wu, H.C., Zhang, S.H., 2006. Stratigraphy, sedimentary structures, and textures of the late Neoproterozoic Doushantuo cap carbonate in South China. J. Sediment. Res. 76 (7), 978–995.
Jiang, GQ, Shi, XY, Zhang, SH, Wang, Y, Xiao, SH, 2011. Stratigraphy and paleogeography of the Ediacaran Doushantuo Formation (ca. 635–551 Ma) in South China. Gondwana Research 19, 831–849.
Jin, C., 2010. Thrust and Decollement System of the Xuefeng Intracontinental Tectonic System. Doctor thesis of Ocean University of China.
Johnson, C.A., Kelley, K.D., Leach, D.L., 2004. Sulfur and oxygen isotopes in barite deposits of the western Brooks Range, Alaska, and implications for the origin of the Red Dog massive sulfide deposits. Econ. Geol. 99 (7), 1435–1448.
Kiyosu, Y., Krouse, H.R., 1990. The role of organic acid in the abiogenic reduction of sulfate and the sulfur isotope effect. Geochem. J. 24, 21–27.
Leach, D.L., Sangster, D.F., Kelley, K.D., Large, R.R., Garven, G., Allen, C.R., Gutzmer, J., 2005. Sediment-hosted lead-zinc deposit: a global perspective. Econ. Geol. 100 (Anniversary Volume), 561–607.
Leng, C.B., Zhang, X.C., Huang, Z.L., Huang, Q.Y., Wang, S.X., Ma, D.Y., Luo, T.Y., Li, C., Li, W.B., 2015. Geology, Re-Os ages, sulfur and lead isotopes of the Diyanqinamu porphyry Mo deposit, Inner Mongolia, NE China. Econ. Geol. 110 (2), 557–574.
Li, B., Hu, B.W., Shi, X.H., Li, J.H., Luo, Q., 2015a. Study on the Silurian sedimentary system of Western Hunan and the formation mode of typical foreland basin. Earth Front. 22 (6), 167–176 (in Chinese with English Abstract).
Li, B., Luo, Q., Hu, B.W., Jin, C.H., 2016. A study on sedimentary environment evolution model of superimposed foreland basin in western Hunan Province. China Petrol. Explor. 21 (6), 81–90 (in Chinese with English Abstract).
Li, C., Cheng, M., Algeo, T.J., Xie, S.C., 2015b. A theoretical prediction of chemical zonation in early oceans (>520 ma). Sci. China Earth Sci. 58 (11), 1901–1909.
Li, C., Love, G.D., Lyons, T.W., Scott, C.T., Feng, L.J., Huang, J., Chang, H.J., Zhang, Q. R., Chu, X.L., 2012. Evidence for a redox stratified cryogenian marine basin, Datangpo Formation, South China. Earth Planet. Sci. Lett. 331–332 (2), 246–256.
Li, C., Love, G.D., Lyons, T.W., Fike, D.A., Sessions, A.L., Chu, X.L., 2010. A stratified redox model for the Ediacaran ocean. Science 328 (5974), 80–83.
Li, X.H., Li, Z.X., Ge, W., Zhou, H., Li, W.X., Liu, Y., Michael, T.D.W., 2003. Neoproterozoic granitoids in South China: crustal melting above a mantle plume at ca. 825 Ma? Precambr. Res. 122 (s 1–4), 45–83.
Li, Z.X., Li, X.H., Kinny, P.D., Wang, J., 1999. The breakup of Rodinia: did it start with a mantle plume beneath south china? Earth Planet. Sci. Lett. 173 (3), 171–181.
Li, X.F., Zhu, Y.T., Xu, J., 2020. Indium as a critical mineral: A research progress report, China. Science Bulletin 65, 3678–3687 (in Chinese with English abstract).
Liang, HY, 1989. Ore material sources of the Longshan gold-antimony deposit. Mineral Deposits 8 (4), 39–48.
Liang, J.C., Liu, Z.K., Li, X.F., Lu, X.P., Meng, L.H., Li, W.J., 2009. Genesis of Laobao Pb-Zn deposit in North Guangxi. J. Guilin Univ. Technol. 29 (2), 161–168 (in Chinese with English abstract).
Liao, S.M., Lu, Q.F., Qin, M.F., Chen, Y.D., Chen, W.L., 2013. Ore-forming mode of Laobao Pb-Zn deposit in Sanjiang, Guangxi Province. Geol. Miner. Resour. South China 29 (1), 54–59 (in Chinese with English abstract).
Liu, H.C., Zhu, B.Q., 1994. Research on the age of Banxi Groups and Lengjiaxi Groups, western Hunan Province. China Science Bulletin 39 (2), 148–150 (in Chinese).
Lott, DA, Coveney, RM, Murowchick, JB, Grauch, RI, 1999. Sedimentary exhalative nickel-molybdenum ores in South China. Economic Geology 94 (7), 1051–1066.
Luo, X.Q., 1990. Geological characteristics and metallogenetic geologic conditions of pyrite and lead-zinc ore-deposits in Yuanling, Hunan Province. Mineral. Petrol. 10 (3), 78–86 (in Chinese with English abstract).
Machel, H.G., Krouse, H.R., Sassen, R., 1995. Products and distinguishing criteria of bacterial and thermochemical sulfate reduction. Appl. Geochem. 10 (4), 373–389.
Marsh, E.E., Hitzman, M.W., Leach, D.L., Critical elements in sediment-hosted deposits (clastic-dominated Zn-Pb-Ag, Mississippi Valley-Type Zn-Pb, sedimentary rock-hosted stratiform Cu, and carbonate-hosted polymetallic deposits): A review. Rev. Econ. Geol., 18, 307-321.
Mei, H.J., Tang, C.J., Li, S.R., Li, Y.M., Zhang, X.C., Lu, D.R., Zhang, L.C., 1998. Lamproites and kimberlites in China and the genesis of diamond deposit. Sci. China 41 (1), 54–92.
Meyer, K.M., Kump, L.R., 2008. Oceanic Euxinia in earth history: causes and consequences. Annual Review of Earth and Planetary Sciences 36, 251–288.
Murakami, H, Ishihara, S, 2013. Trace elements of indium-bearing sphalerite from tin-polymetallic deposits in Bolivia, China and Japan: a femto-second LA-ICPMS study. Ore Geology Reviews 53, 223–243.
Ohmoto, H., 1972. Systematics of sulfur and carbon isotopes in hydrothermal ore deposits. Econ. Geol. 67, 551–578.
Peng, J.T., Hu, R.Z., Zhao, J.H., Fu, Y.Z., Lin, Y.X., 2003. Scheelite Sm-Nd dating and quartz Ar-Ar dating for Woxi Au-Sb-W deposits, western Hunan. Chin. Sci. Bull. 48 (23), 2640–2646.
Robinson, B.W., Kusakabe, M., 1975. Quantitative preparation of sulfur dioxide for $^{32}S/^{34}S$ analyses from sulfides by combustion with cuprous oxide. Anal. Chem. 47 (7), 1179–1181.
Schneider, J., Boni, M., Lapponi, F., Bechstadt, T., 2002. Carbonate-Hosted zinc-lead deposits in the lower Cambrian of Hunan, South China: A radiogenic (Pb, Sr) isotope study. Econ. Geol. 1815–1827.
Schwartz, M.O., 2000. Cadmium in zinc deposits: economic geology of a polluting element. Int. Geol. Rev. 42, 445–469.
Schwarz-Schampera, U., Herzig, P.M., 2002. Indium: Geology, Mineralogy, and Economics. Springer-Verlag, Berlin.
Shields, G.A., 2005. Neoproterozoic cap carbonates: a critical appraisal of existing models and the plumeworld, hypothesis. Terra Nova 17 (4), 299–310.
Shu, L.S., 2012. An analysis of principal features of tectonic evolution in South China Block. Geol. Bull. China 31, 1035–1053 (in Chinese with English abstract).
Simons, B., Andersen, J.C., Shail, R.K., Jenner, F.E., 2017. Fractionation of Li, Be, Ga, Nb, Ta, In, Sn, Sb, W and Bi in the peraluminous Early Permian Variscan granites of the

Cornubian Batholith: precursor processes to magmatic-hydrothermal mineralisation. Lithos 278–281, 491–512.
Sinclair, W.D., Kooiman, G.J.A., Martin, D.A., Kjarsgaard, I.M., 2006. Geology, geochemistry and mineralogy of indium resources at Mount Pleasant, New Brunswick, Canada. Ore Geology Reviews 28 (1), 123–145.
Stillings LL, 2017, Selenium, chap. Q of Schulz KJ, DeYoung, JH. Jr., Seal RR II, Bradley DC, eds., Critical mineral resources of the United States—Economic environmental geology prospects for future supply: U.S. Geological Survey Professional Paper, 1802, Q1–Q55.
Su, JB, Dong, SW, Zhang, YQ, Li, Y, Chen, XH, Ma, LC, Chen, JS, 2017. Orogeny processes of the western Jiangnan Orogen, SouthChina:Insights from Neoproterozoic igneous rocks and a deep seismicprofile. Journal of Geodynamics 103, 42–56.
Tu, G.C., 2002. Two unique mineralization areas in southwest China. Bull. Mineral. Petrol. Geochem. 21 (1), 1–2 (in Chinese).
Wan, J.M., 1986. Geochemical studies of the Xi'an Tungsten ore deposit, west Hunan, China. Geochemica 2, 183–192 (in Chinese with English abstract).
Wang, H.Y., Shi, J.X., 1997. Sources of ore-forming materials and controls over depositional differentiation in the epithermal mineralization series in the Danzhai-Sandu-Duyun area of Guizhou province. Acta Miner. Sin. 17, 491–500 (in Chinese with English abstract).
Wang, J., Li, Z.X., 2003. History of Neoproterozoic rift basins in South China: implications for Rodinia break-up. Precambr. Res. 122 (1–4), 141–158.
Wang, J.S., Wen, H.J., Li, C., Ding, W., Zhang, J.R., 2011. Re-Os isotope dating of arsenopyrite from the quartz vein-type gold deposit, Southeastern Guizhou provience, and its geological implications. Acta Geol. Sin. 85 (6), 955–964 (in Chinese with English abstract).
Wang, X.L., Zhao, G.C., Zhou, J.C., Liu, Y.S., Hu, J., 2008. Geochronology and Hf isotopes of zircon from volcanic rocks of the Shuangqiaoshan Group, South China: implications for the Neoproterozoic tectonic evolution of the eastern Jiangnan Orogen. Gondwana Res. 14, 355–367.
Wang, X.L., Zhou, J.C., Qiu, J.S., Gao, J.F., 2004. Geochemistry of the Meso- to Neoproterozoic basic-acid rocks from Hunan province, South China: implications for the evolution of the western Jiangnan Orogen. Precambr. Res. 135, 79–103.
Wang, Y.J., Wu, C.M., Zhang, A.M., Fan, W.M., Zhang, Y.H., Zhang, Y.Z., Peng, T.P., Yin, C.Q., 2012. Kwangsian and Indosinian reworking of the eastern South China Block: Constraints on zircon U-Pb geochronology and metamorphism of amphibolites and granulites. Lithos 150, 227–242. https://doi.org/10.1016/j.lithos.2012.04.022.
Wedepohl, K.H., 1995. The Composition of the Continental Crust. Geochim. Cosmochim. Acta 59 (7), 1217–1232.
Wen, H.J., Zhou, Z.B., Liu, L., Qin, C.J., Huang, Y.C., Wen, X.Q., Shi, Q.P., Xu, D.P., Wang, W.J., 2017. The discovery of the Dahebian Pb Zn deposit in Tianzhu area of Guizhou Province and its prospecting significance. Geol. Bull. China 36 (7), 1288–1293 (in Chinese with English abstract).
Wen, H.J., Fan, H.F., Tian, S., Wang, Q., Hu, R., 2016a. The formation conditions of the early Ediacaran cherts, South China. Chem. Geol. 430, 45–69.
Wen, H.J., Carignan, J., 2011. Selenium isotopes trace the source and redox processes in the black shale-hosted Se-rich deposits in China. Geochim. Cosmochim. Acta 75 (6), 1411–1427.
Wen, H.J., Zhu, C.W., Zhang, Y.X., Cloquet, C., Fan, H.F., Fu, S.H., 2016b. Zn/Cd ratios and cadmium isotope evidence for the classification of lead-zinc deposits. Sci. Rep. 6, 25273. https://doi.org/10.1038/srep25273.
Werner, T.T., Mudd, G.M., Jowitt, S.M., 2017. The world's by-product and critical metal resources part iii: a global assessment of indium. Ore Geol. Rev. 86, 939–956.
Wilkinson, J.J., 2014. Sediment-hosted zinc–lead mineralization: processes and perspectives. Treat. Geochem. 219–249.
Wu, Y, Kong, ZG, Chen, MH, Zhang, CQ, Cao, L, Tang, YJ, Yuan, X, Zhang, P, 2019. Trace elements in sphalerites from the Mississippi Valley-type lead-zinc deposits around the margins of Yangtze Block and its geological implications: A LA-ICPMS study. Acta Petrologica Sinica 35 (11), 3443–3460.
Xiang, H., Luo, C.J., 2013. Discussion on the ore-forming geological features, ore-controlling factors and prospecting direction of the Chenxi-Yuanling pyrite and Pb-Zn mineralization clusters in Western Hunan Province. Geol. Miner. Resour. South China 29 (1), 28–36 (in Chinese with English abstract).
Xia, F., Ma, D., Pan, J., Sun, Z., Cao, S., Nie, W., Wu, K., 2004. Strontium isotope evidence for hydrothermal-sedimentary for Tianzhu Dahebian and Yuping barite deposits. Guizhou Province. Science Bulletin 49 (24), 2592–2595 (in Chinese with English abstract).
Xu, J., Cook, N.J., Ciobanu, C.L., et al. 2020. Indium distribution in sphalerite from sulfide–oxide–silicate skarn assemblages: a case study of the Dulong Zn–Sn–In deposit, Southwest China. Mineral. Deposita. 10.1007/s00126-020-00972-y.
Xu, L.G., Lehmann, B., Mao, J.W., Qu, W.J., Du, A.D., 2011. Re-Os age of polymetallic Ni-Mo-PGE-Au mineralization in Early Cambrian balck shales of South China: a reassessment. Econ. Geol. 106, 511–522.
Xu, L, Luo, CG, Wen, HJ, Zhou, ZB, Qin, CJ, 2018. Origin of ore-forming fluids of the Zn-Pb-(Cu) deposits in the Jinbao mine district of eastern Guizhou Province, China: Evidence from Chemical Compositions of Fluid Inclusions and their Lithium Isotopes. Geochemical Jorunal 52, 483–496.
Yang, Z.W., Liu, L., Liao, L.P., Qin, C.J., Wen, H.J., 2015. Discussion on stable isotope characteristics and the source of mineral material in the Jinbao lead-zinc deposit in Zhenyuan County, Southeastern Guizhou province, China. Acta Mineral. Sin. 35 (2), 147–153 (in Chinese with English abstract).
Ye, L, Cook, NJ, Ciobanu, CL, Liu, YP, Zhang, Q, Liu, TG, Gao, W, Yang, YL, Danyushevsky, L, 2011. Trace and minor elements in sphalerite from base metal deposits in South China: A LA-ICPMS study. Ore Geology Reviews 39, 188–217.
Ye, L., Cook, N.J., Liu, T.G., Ciobanu, C.L., Gao, W., Yang, Y., 2012. The Niujiaotang Cd-rich zinc deposit, Duyun, Guizhou province, Southwest China: ore genesis and mechanisms of cadmium concentration. Miner. Deposita 47 (6), 1–18.
Ye, L., Hu, Y.S., Yang, S.P., Wei, C., Yang, X.Y., Li, Z.L., An, Q., Lu, M.D., 2018. A discussion on the Pb-Zn mineralization of the Qiandong metallogenic belt. Acta Mineral. Sin. 38 (6), 709–715 (In Chinese with English Abstract).
Zartman, R.E., Doe, B.R., 1981. Plumbotectonics—the model. Tectonophysics 75, 135–162.
Zeng, Y., Li, C.J., 2007. Discussion on the geological characteristics and sources of ore-forming materials of Dongjiahe Pb-Zn deposit in western Hunan Province. Geol. Miner. Resour. South China 3, 24–30 (in Chinese with English abstract).
Zhang, H., Xie, Y., Zhang, C.H., et al., 2013a. The discussion on the sedimentary characteristics and structural properties of Lengjiaxi Group in the west of Jiangnan orogenic belt. Earth Sci. Front. 20 (6), 269–281.
Zhang, G.W., Guo, A.L., Wang, Y.J., Li, S.Z., Dong, Y.P., Liu, S.F., He, D.F., Cheng, S.Y., Lu, R.K., Yao, A.P., 2013b. Tectonics of South China Continent and its implications. Sci. China Earth Sci. 56 (11), 1804–1828.
Zhang, W.L., Che, X.D., Chen, W.D., Wang, R.C., Zhang, D., 2017. A new potential Caledonian-Indosinian ore concentration area: evidence from diagenesis and mineralization ages of the Miao'ershan-Yuechengling region. Acta Geol. Sin. (English Edition) 91 (2), 743–744.
Zhao, G.C., 2015. Jiangnan Orogen in South China: Developing from divergent double subduction. Gondwana Res. 27, 1173–1180.
Zhao, G.C., Cawood, P.A., 2012. Precanbrian geology of China. Precambr. Res. 222–223, 13–54.
Zheng, Y.F., 1990. The effect of Rayleigh degassing of magma on sulfur isotope composition: a quantitative evalution. Terra Nova 2 (1), 74–78.
Zhou, M.Z., Luo, T.Y., Liu, S.R., et al., 2013a. SHRIMP zircon age for a K-bentonite in the top of the Laobao Formation at the Pingyin section, Guizhou, South China. Sci. China Earth Sci. https://doi.org/10.1007/s11430-013-4604-7.
Zhou, M.Z., Luo, T.Y., Liu, S.R., et al., 2013b. SHRIMP zircon age for a K-bentonite in the top of the Laobao Formation at the Pingyin section, Guizhou, South China. Sci. China Earth Sci. 43 (7), 1195–1206. https://doi.org/10.1007/s11430-013-4604-7.
Zhou, Y., 2017. Metallogenesis Study of Huayuan MVT type Pb-Zn Ore Concentration Area, Hunan. Doctor thesis of Chengdu University of Technology, Chengdu.
Zhou, C, Bao, H, Peng, Y, Yuan, X, 2010. Timing the deposition of ^{17}O-depleted barite at the aftermath of Nantuo glacial meltdown in South China. Geology 38 (10), 903–906.
Zhou, Y., Duan, Q.F., Liang, C., Fang, L., Huang, H.L., 2014. Large-scale low-temperature mineralizations in Western Hunan-Western Hubei lead-zinc deposits. Geol. J. China Univ. 20 (2), 198–212 (in Chinese with English abstract).
Zhou, Z.B., Wen, H.J., 2021. A magmatic-hydrothermal indium-bearing polymetallic vein mineralization belt in the western Jiangnan Orogen: Evidence from zinc and cadmium isotopes of sphalerite. Ore Geol. Rev. 131, 103843.
Zhou, Z.B., Wen, H.J., Qin, C.J., et al., 2018. The genesis of the Dahebian Zn-Pb deposit and associated barite mineralization: Implications for hydrothermal fluid venting events along the Nanhua Basin, South China. Ore Geol. Rev. 101, 785–802.
Zhou, Z.B., Wen, H.J., Qin, C.J., Liu, L., 2017. Geochemical and isotopic evidence for a magmatic-hydrothermal origin of the polymetallic vein-type Zn-Pb deposits in the northwest margin of Jiangnan Orogen, South China. Ore Geol. Rev. 86, 673–691.